© 2022. Published by The Company of Biologists Ltd | Journal of Cell Science (2022) 135, jcs259114. doi:10.1242/jcs.259114

RESEARCH ARTICLE

Reciprocal regulation of p21 and Chk1 controls the cyclin D1-RB pathway to mediate senescence onset after G2 arrest

Gérald Lossaint[1,*,¶], Anđela Horvat[2,¶], Véronique Gire[3], Katarina Bačević[1], Karim Mrouj[1,‡], Fabienne Charrier-Savournin[3,§], Virginie Georget[3,4], Daniel Fisher[1] and Vjekoslav Dulić[1,]**

ABSTRACT

Senescence is an irreversible withdrawal from cell proliferation that can be initiated after DNA damage-induced cell cycle arrest in G2 phase to prevent genomic instability. Senescence onset in G2 requires p53 (also known as TP53) and retinoblastoma protein (RB, also known as RB1) family tumour suppressors, but how they are regulated to convert a temporary cell cycle arrest into a permanent one remains unknown. Here, we show that a previously unrecognised balance between the cyclin-dependent kinase (CDK) inhibitor p21 and the checkpoint kinase Chk1 controls cyclin D–CDK activity during G2 arrest. In non-transformed cells, p21 activates RB in G2 by inhibiting cyclin D1 complexed with CDK2 or CDK4. The resulting G2 exit, which precedes the appearance of senescence markers, is associated with a mitotic bypass, Chk1 downregulation and reduction in the number of DNA damage foci. In p53/RB-proficient cancer cells, a compromised G2 exit correlates with sustained Chk1 activity, delayed p21 induction, untimely cyclin E1 re-expression and genome reduplication. Conversely, Chk1 depletion promotes senescence by inducing p21 binding to cyclin D1– and cyclin E1–CDK complexes and downregulating CDK6, whereas knockdown of the checkpoint kinase Chk2 enables RB phosphorylation and delays G2 exit. In conclusion, p21 and Chk2 oppose Chk1 to maintain RB activity, thus promoting the onset of senescence induced by DNA damage in G2.

KEY WORDS: Senescence, DNA damage, G2 arrest, Cyclin D, RB, p21, Chk1, CDK6

INTRODUCTION

Senescence is essentially a permanent withdrawal from cell proliferation that can be induced by diverse stimuli such as dysfunctional telomeres, DNA damage, excessive mitogenic signalling or oncogene activation (Di Micco et al., 2021). Senescent cells are characterized by hypertrophy, intense metabolic activity, increased β-galactosidase (SA-β-gal, also known as GLB1) activity, chromatin remodelling and enhanced secretion of proinflammatory molecules, known as the senescence-associated secretory phenotype (SASP; Sharpless and Sherr, 2015; Roger et al., 2021). In addition to preventing neoplastic transformation, senescence plays an important role in a number of physiological and pathological processes contributing to age-related disorders and cancer (Di Micco et al., 2021; He and Sharpless, 2017).

Irreversible cell cycle arrest precedes the appearance of the routinely used markers of senescence (SA-β-gal), and it requires functional p53 (also known as TP53) and retinoblastoma protein (RB, also known as RB1) family tumour suppressors (Sharpless and Sherr, 2015). In replicative senescence, G1 arrest is mediated by the p53-induced cyclin-dependent kinase (CDK) inhibitor $p21^{Waf1/Cip1}$ (p21, or CDKN1A), which inhibits CDKs bound to the G1 cyclins D1 and E1 (CycD1 and CycE1, encoded by *CCND1* and *CCNE1*, respectively), thereby blocking the inactivating phosphorylation of the RB family of pocket proteins and preventing DNA replication (Dulić et al., 2000; Stein et al., 1999). This stable G1 arrest does not require the CDK4/CDK6 inhibitor $p16^{INK4A}$ (p16, or CDKN2A), which accumulates only in late stages of senescence and ensures its irreversibility by preventing formation of CycD1–CDK4/CDK6 complexes (Alcorta et al., 1996; He and Sharpless, 2017; Ito et al., 2018; Sharpless and Sherr, 2015; Stein et al., 1999).

Senescence can also be triggered in the G2 phase of the cell cycle (Gire and Dulić, 2015; Shaltiel et al., 2015). DNA damage-induced G2 arrest is initiated by ATM/ATR-mediated phosphorylation of the checkpoint kinases Chk1 and Chk2 (encoded by *CHEK1* and *CHEK2*, respectively), which, by inhibiting CDC25 phosphatases, block activation of the mitosis inducer CDK1 (Chen and Poon, 2008). Converting a temporary G2 arrest into a permanent cell cycle arrest, termed 'G2 exit', which precedes the full appearance of senescence phenotype markers, requires p21. In addition to inhibiting CycA–CDK1/CDK2 (Bačević et al., 2017a; Baus et al., 2003; Lossaint et al., 2011), thereby preventing CycB1–CDK1 activation (Lemmens and Lindqvist, 2019), p21 sequesters inactive CycB1–CDK1 in the nucleus (Charrier-Savournin et al., 2004; Krenning et al., 2014). This leads to downregulation of CycB1 and other mitotic regulators (Charrier-Savournin et al., 2004; Lossaint et al., 2011) via APC/C^{Cdh1}-mediated degradation (Shaltiel et al., 2015). The G2 exit, which probably corresponds to the onset of senescence, is preceded by a mitotic bypass, giving rise to stably arrested tetraploid G1 cells (Gire and Dulić, 2015; Johmura et al., 2014; Krenning et al., 2014). Additionally, p21 inhibits phosphorylation of the RB family of pocket proteins (Baus et al., 2003; Johmura et al., 2014) that leads to the repression of E2F-dependent G2/M regulators (Jackson et al., 2005; Johmura et al., 2014; Sadasivam and DeCaprio, 2013). However, the identity of the RB kinase(s) that are targeted by p21 to trigger G2 exit has not been established. While CycD1-associated CDK4 and CDK6 promote

[1]IGMM, University of Montpellier, CNRS, 34293 Montpellier, France. [2]Division of Molecular Medicine, Ruđer Bošković Institute, 10000 Zagreb, Croatia. [3]CRBM, University of Montpellier, CNRS, 34293 Montpellier, France. [4]Montpellier Ressources Imagerie, BioCampus, University of Montpellier, CNRS, INSERM, 34293 Montpellier, France.
*Present address: Institut du cancer de Montpellier, 34090 Montpellier, France.
‡Present address: Institute for Stem Biology and Regenerative Medicine, Stanford University School of Medicine, Stanford, CA 94305, USA.
§Present address: PerkinElmer, Inc., Parc Marcel Boiteux, BP 84175, 30200 Codolet, France.
¶These authors contributed equally to this work

**Author for correspondence (vjekoslav.dulic@igmm.cnrs.fr)

V. Gire, 0000-0002-9009-2185; K.B., 0000-0003-3919-2858; K.M., 0000-0002-8066-9833; V. Georget, 0000-0002-6998-3100; D.F., 0000-0002-0822-3482; V.D., 0000-0003-1201-3901

Handling Editor: David Glover
Received 12 July 2021; Accepted 18 March 2022

Journal of Cell Science (2022) 135, jcs259114. doi:10.1242/jcs.259114

G1/S progression by phosphorylating and inactivating RB (Chung et al., 2019; Topacio et al., 2019), the role of the CycD1–RB module after the restriction point remains understudied. Unlike CycE1, CycD1 is also expressed in late cell cycle phases (Chassot et al., 2008; Gookin et al., 2017; Hitomi and Stacey, 1999; Matsushime et al., 1994; Yang et al., 2006). It is therefore possible that, like at the G1/S transition (Lundberg and Weinberg, 1998), CycD1–CDKs 'prime' RB, enabling further phosphorylation by CDK2 and/or CDK1. This is consistent with a CycD1 role as a sensor or effector of anti-proliferative cues in cells, where its G2 levels control the decision between proliferation and quiescence (Min et al., 2020; Yang et al., 2017b). However, whether the CycD1–RB module senses DNA damage in G2 has not been investigated.

Permanent G2 exit has been proposed to serve as a safeguard mechanism to prevent adaptation to the G2/M checkpoint (Baus et al., 2003), i.e. passage into mitosis of cells with damaged DNA, which can occur in cells lacking sufficient Chk1 activity (Feringa et al., 2018; Shaltiel et al., 2015). G2/M checkpoint adaptation also occurs in the absence of p53 or p21, and subsequent cytokinesis failure can lead to accumulation of polyploid nuclei or cell death (Bunz et al., 1998; Johmura et al., 2014). Alternatively, in p53-deficient cells experiencing persistent telomere dysfunction, a prolonged G2 arrest entails mitotic bypass and genome reduplication (Davoli et al., 2010), generating genomic instability (Davoli and de Lange, 2012), and coincides with sustained Chk1 and Chk2 activity. These results imply that, like p21, Chk1/Chk2 kinases stabilise the G2 arrest following continuous DNA damage, and suggest a certain redundancy between ATM/p53/p21 and ATM/ATR/Chk1/Chk2 pathways. They also show that a stable G2 arrest is not equivalent to and does not necessarily lead to a G2 exit. Paradoxically, although recent work has implicated ATR/Chk1 in senescence onset in G2 (Feringa et al., 2018; Johmura et al., 2016), DNA damage-induced senescence or terminal differentiation are all invariably associated with Chk1 downregulation (Gabai et al., 2008; Gottifredi et al., 2001; Gire, 2004; Lossaint et al., 2011; Park et al., 2015; Ullah et al., 2011). It is currently unclear whether the shutdown of Chk1 signalling is required for the permanent cell cycle arrest or is merely a consequence.

In this study, we investigated the kinase network that controls the transition between DNA damage-induced G2 arrest and permanent G2 exit preceding senescence. We found that in non-transformed cells, the G2 exit is driven by p21-dependent inhibition of CycD1–CDK complexes, which blocks RB phosphorylation and coincides with Chk1 but not Chk2 downregulation. We further show that sustained Chk1 activation in cancer cells is associated with impaired G2 exit and endoreplication, whereas its acute depletion strongly accelerated permanent cell cycle exit via p21-mediated inhibition of RB kinases. Our results suggest that, due to opposing regulation of RB phosphorylation, Chk1 inhibits, whereas p21 and Chk2 promote, the onset of senescence in G2. Finally, we uncover CDK6 downregulation as an important component of the CycD1-RB pathway control during DNA damage-induced cell cycle exit in cancer cells.

RESULTS

CycD1 and CycE1 accumulate upon DNA damage-induced G2 arrest prior to cell cycle exit and senescence

RB and p21 play key roles both in senescence (Chicas et al., 2010; Herbig et al., 2004; Yosef et al., 2017; Sturmlechner et al., 2021) and in DNA damage-induced permanent cell cycle arrest in G2 (Baus et al., 2003; Johmura et al., 2014). As such, the p21-mediated inhibition of RB kinases might be a key event triggering the switch between temporary and permanent G2 arrest (hereafter G2 exit) that precedes senescence onset. We have shown previously that in human diploid fibroblasts (HDFs), CycD1 is expressed after the G1/S transition (Chassot et al., 2008) and we find that this coincides with increased CycD1–CDK-specific RB phosphorylation at Ser780 (Fig. 1A; P^{S780}; Geng et al., 2001; Kitagawa et al., 1996). Moreover, CycD1 levels specifically decrease upon serum depletion after G1/S-phase transition, coinciding with the appearance of hypophosphorylated RB (Fig. 1A). Thus, we surmised that the CycD1–RB module could serve as a sensor for anti-proliferative cues even in late cell cycle phases. We therefore investigated whether p21 inhibits RB phosphorylation and promotes DNA damage-induced senescence onset in G2 by targeting CycD1–CDK complexes.

To test this hypothesis, we exposed HDFs to genotoxic drugs, previously shown to induce G2 exit: ICRF-193, a DNA topoisomerase II inhibitor, which generates double-strand DNA breaks in G2 phase, or bleomycin, a radiomimetic drug that causes G1 or G2 arrest (Fig. S1A; Baus et al., 2003). After 48 h, both drugs inhibited RB phosphorylation and reduced RB levels (Broude et al., 2007), downregulated cyclin A (CycA) and Ki67, and induced accumulation of p21 and hypophosphorylated p130 (also known as RB2), a member of the dimerization partner, RB-like, E2F and multi-vulval class B (DREAM) complex (Sadasivam and DeCaprio, 2013; Fig. 1B–D). These hallmarks of permanent cell cycle arrest, observed also upon irradiation and in replicative senescence (Fig. 1B,E), invariably preceded the later appearance of senescent markers such as an increase in nuclear size (Fig. 1F), upregulation of the CDK4/6 inhibitor p16 and positive SA-β-gal staining (Fig. 1E,F; Fig. S1B,C). This shows that cell cycle exit precedes and is not equivalent to senescence. In addition, both G1 and G2 cell cycle arrests led to accumulation of CycE1 and CycD1, which is also observed in senescent cells (Fig. 1B,E; Dulić et al., 1993). Whereas CycE1 accumulated in p21-bound complexes only after CycA degradation as a result of mitotic bypass (Fig. 1B,E; Fig. S1D), single-cell immunofluorescence analysis showed that CycD1 had already increased in G2-arrested cells, as documented by co-expression with CycA and CycB1 (Fig. 1G,H; Fig. S1E,F). Thus, cyclin D1 stabilization after G2 arrest might be an early marker of the G2 exit.

p21 targets CycD1 to inhibit RB phosphorylation and promote senescence onset after G2 arrest

Next, we asked whether p21 targets CycD1–CDK complexes in G2-arrested cells, thereby inhibiting RB phosphorylation. Indeed, as shown by immunofluorescence (Fig. 2A–D) and immunoblots of p21 and CycD1 immunoprecipitates (Fig. 2E,F), the G2 arrest correlated with increasing co-expression and binding of both CycD1 and CycA with p21 (Fig. 2E,F). Interestingly, in addition to CycD1–CDK4, G2-arrested cells also accumulated CycD1–CDK2 complexes (Fig. 2F), which also accumulate in senescent fibroblasts (Dulić et al., 1993; Stein et al., 1999). These data show that p21 simultaneously binds CycA–CDK1/2 complexes that drive mitosis, and CycD1–CDK2/4/6 complexes, that phosphorylate RB. Consequently, preventing p21 induction might stimulate CycD1-dependent RB phosphorylation after G2 arrest. Indeed, CycD1–CDK-specific RB phosphorylation (P^{S780}) was promoted by p21 knockdown (KD) in HDFs and human mammary epithelial cells (HMECs; Fig. 2G) or by expression of the human papillomavirus type 16 (HPV16)-E6 oncoprotein (Fig. S2A), which degrades p53 and prevents p21 induction (Baus et al., 2003) thereby compromising the cell cycle exit (Fig. S2B,C). Moreover, p21 KD

Journal of Cell Science (2022) 135, jcs259114. doi:10.1242/jcs.259114

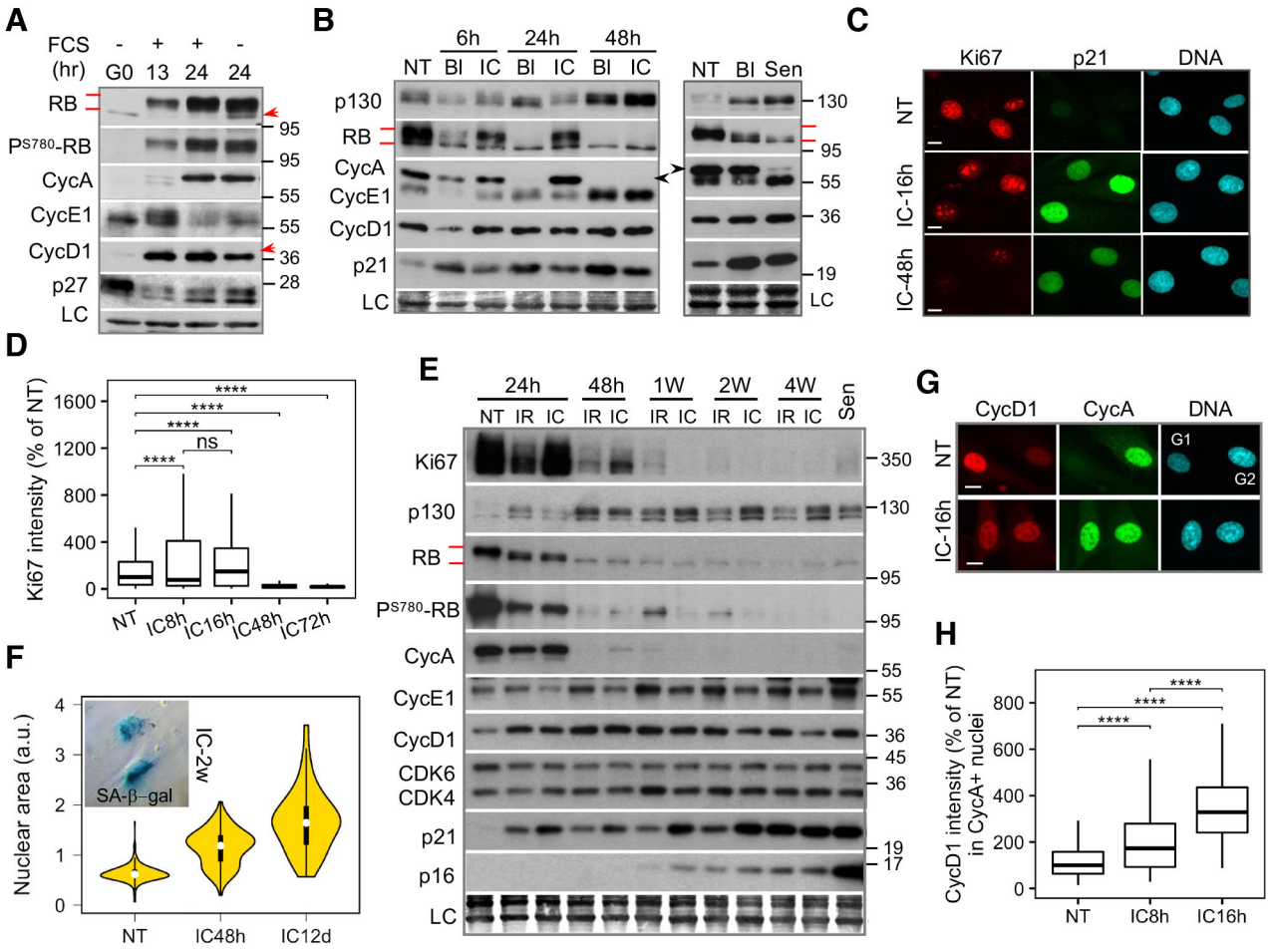

Fig. 1. CycD1 and CycE1 accumulate upon DNA damage-induced G2 arrest prior to cell cycle exit and senescence. (A) Immunoblots showing RB levels, CycD1–CDK-specific RB phosphorylation (P^{S780}-RB) and expression of different cyclins in HDFs released from quiescence (G0) by serum addition (+FCS) (*n*=2). For the 24 h timepoint, FCS was removed after 13 h. Red arrows indicate hypophosphorylated RB and reduced CycD1 levels in the absence of FCS. LC, loading control. (B) Immunoblots showing cyclins, p21, RB and p130 after DNA damage-induced cell cycle exit (left panel) and in HDFs that underwent replicative senescence (Sen, right panel). HDFs were incubated with bleomycin (BI) or ICRF-193 (IC) for the indicated times (left panel) and for 12 h (right panel) (*n*=4). Sen: population doubling (PD) 74. NT, non-treated cells. Arrows indicate CycA bands. LC, loading control. (C) Representative immunofluorescence images showing co-expression of Ki67 and p21 in non-treated (NT) HDFs and HDFs incubated with ICRF-193 (IC) for 16 and 48 h (*n*=3). Scale bars: 10 µm. (D) Quantification of Ki67 intensity in immunofluorescence images from HDFs incubated with ICRF-193 (IC) for the indicated durations (expressed as a percentage of Ki67 intensity in NT). Cells were pooled from four independent experiments. More than 100 cells were analysed in each experiment. NT, non-treated cells. (E) Immunoblots showing changes in the indicated cell cycle regulators, RB levels and CycD1-specific phosphorylation (P^{S780}-RB) in HDFs exposed to ionizing γ-irradiation (IR, 10 Gy) or treated with ICRF-193 (IC) for the indicated times (*n*=3). NT, non-treated cells; Sen, senescent cells. LC, loading control. (F) Violin plots showing nuclear size in non-treated (NT) HDFs and HDFs treated with ICRF-193 for 48 h and 12 days. More than 200 cells were analysed in each experiment (*n*=3). a.u., arbitrary units. Insert: phase contrast images showing β-galactosidase staining of HDFs incubated with ICRF-193 (IC) for two weeks. (G) Representative immunofluorescence images (*n*=3) showing co-expression of CycD1 and CycA in non-treated (NT) HDFs and HDFs treated with ICRF-193 (IC) for 16 h. Scale bars: 10 µm. (H) Quantification of cyclin D1 intensity in cyclin A-positive nuclei in non-treated (NT) HDFs and HDFs exposed to ICRF-193 (IC) for 8 or 16 h (expressed as a percentage of CycD1 intensity in NT). Cells (>200) were pooled from three independent experiments. For box plots in D,H, the box represents the 25–75th percentiles, central line indicates the median, and whiskers indicate the 10th and 90th percentiles. ns, not significant, ****$P \leq 0.0001$; two-tailed unpaired *t*-test. In all immunoblots, loading controls (LC) were Amido Black-stained membranes. Red bars indicate RB phosphorylation shift.

prevented DNA damage-induced upregulation of CycD1 (Fig. 2G) and, consequently, accumulation of CycD1–CDK2/4/6 complexes in G2-arrested cells (Fig. 2H). While these results are in agreement with the proposed role of p21 in stabilizing CycD1 (Chen et al., 2013) and confirm p21-dependent inhibition of CycD1–CDK-specific RB phosphorylation, they might also link accumulation of p21–CycD1–CDK complexes to G2 exit and senescence onset.

To further corroborate the role of CycD1–CDK complexes in phosphorylating RB beyond the G1/S transition, we knocked down CycD1 in proliferating HDFs. Indeed, in cycling cells, CycD1 KD strongly reduced expression and phosphorylation of both RB and p130 despite unchanged CycE1 and CycA levels (Fig. 2I), suggesting that the CDK2 associated with these cyclins cannot compensate for RB phosphorylation by CycD1–CDK complexes. Indeed, CycE1 KD failed to reduce CycD1–CDK-specific RB phosphorylation on Ser780 and little affected overall RB and p130 phosphorylation in cycling cells (Fig. 2I). Moreover, CycD1 KD also reduced p21 induction by ICRF-193 (Fig. 2I, IC-48 h), which is consistent with CycD1–CDK complexes being major p21 targets after DNA damage.

Finally, to validate the key role of RB in the DNA damage-induced G2 arrest to G2 exit transition, we conditionally expressed

Journal of Cell Science (2022) 135, jcs259114. doi:10.1242/jcs.259114

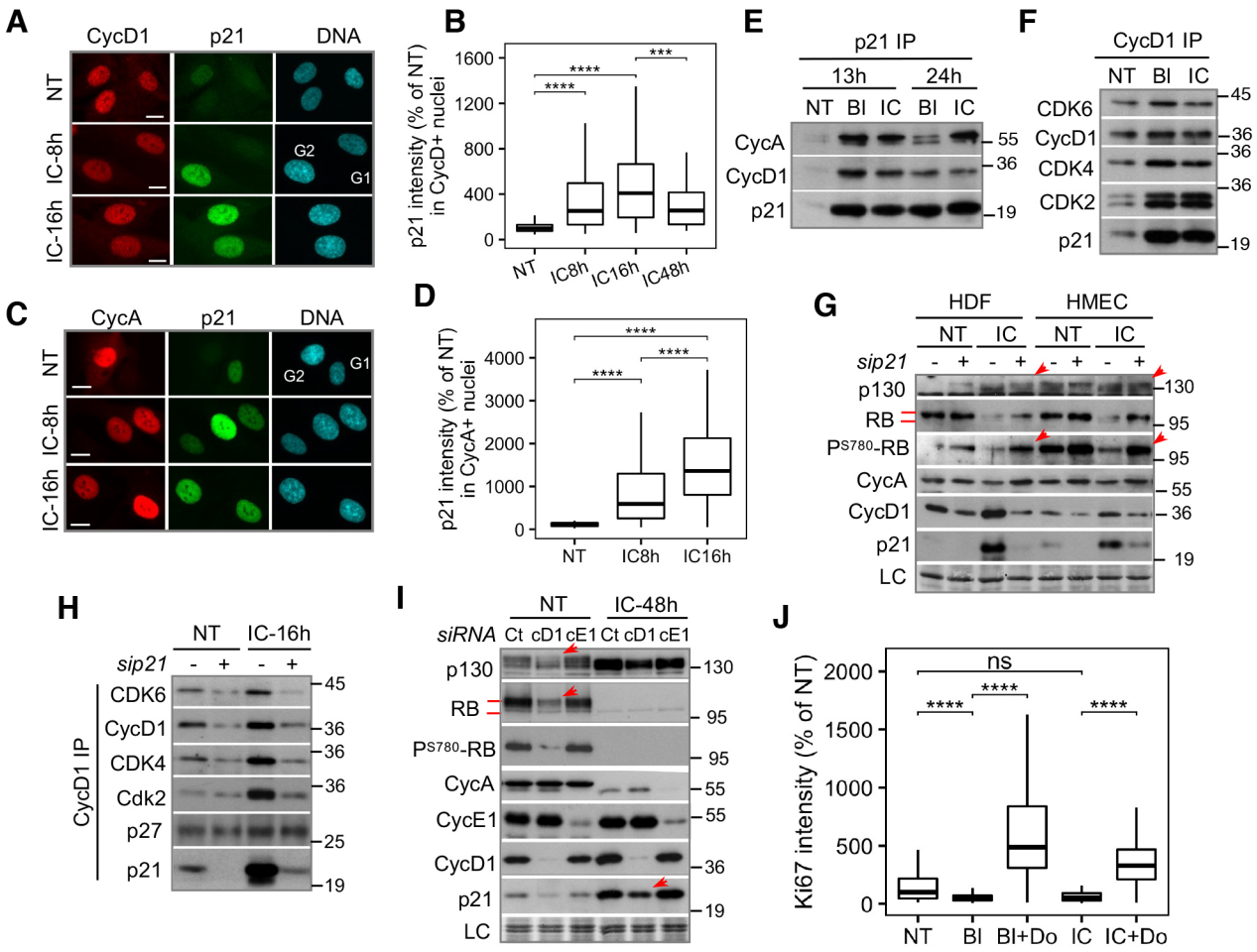

Fig. 2. p21 targets CycD1 to inhibit RB phosphorylation and promote senescence onset after G2 arrest. (A) Representative immunofluorescence images (*n*=3) showing p21 and CycD1 co-localization in non-treated (NT) HDFs and HDFs incubated with ICRF-193 (IC) for the indicated times. Scale bars: 10 µm. (B) Quantification of p21 intensity in CycD1-positive nuclei in non-treated (NT) HDFs and HDFs incubated with ICRF-193 (IC) for the indicated times (expressed as a percentage of p21 intensity in NT). Cells (>200) were pooled from three independent experiments. (C) Representative immunofluorescence images (*n*=2) showing co-localization of CycA and p21 in HDFs incubated with ICRF-193 (IC) for the indicated times. Scale bars: 10 µm. (D) Quantification of p21 intensity in CycA-positive nuclei in HDFs incubated with ICRF-193 for the indicated times. Cells (>100) were pooled from two independent experiments. (E) Immunoblots showing CycD1 and CycA levels in p21 immunoprecipitates (IP) from extracts of non-treated (NT) HDFs or HDFs incubated with bleomycin (BI) or ICRF-193 (IC) for the indicated times (*n*=2). (F) Immunoblots showing p21 and CDK levels in CycD1 immunoprecipitates (IP) in lysates from non-treated (NT) HDFs and HDFs incubated with bleomycin (BI) or ICRF-193 (IC) for 16 h (*n*=2). (G) Immunoblots showing the effects of p21 depletion (sip21) on CycD1, CycA, p130 and RB levels, and CycD1–CDK-specific RB phosphorylation (P^{S780}) levels in extracts from non-treated (NT) HDFs and HMECs or cells incubated with ICRF-193 (IC) for 16 h (*n*=2). Red arrows show increased p130 phosphorylation (shifted band) and P^{S780}-RB after p21 KD (+). LC, loading control. (H) Immunoblots of the indicated proteins in CycD1 immunoprecipitates (IP) from extracts of non-treated (NT) HDFs or HDFs exposed to ICRF-193 (IC) for 16 h that were previously depleted (+) or not (–) for p21 (sip21) (*n*=2). (I) Immunoblots showing effects of CycD1 (cD1) and CycE1 (cE1) knockdown on p21, CycA, p130 and RB levels and CycD1–CDK-specific RB phosphorylation (P^{S780-}-RB) in non-treated (NT) HDFs and HDFs exposed to ICRF-193 (IC) for 48 h (*n*=2). Ct, siRNA control. LC, loading control. Red arrows show reduced p130, RB and p21 levels after CycD1 KD. (J) Quantification of Ki67 intensity in T_{121}-expressing fibroblasts exposed to bleomycin (BI) or ICRF-193 (IC) for 48 h (expressed as a percentage of Ki67 intensity in NT). Doxycycline (Do) was added 12 h before incubation with genotoxic agents. Cells (>100) were pooled from two independent experiments. NT, non-treated cells. For box plots in B,D,J, the box represents the 25–75th percentiles, central line indicates the median, and whiskers indicate the 10th and 90th percentiles. ns, not significant, ***$P\leq0.001$, ****$P\leq0.0001$; two-tailed unpaired *t*-test. In all immunoblots, loading controls (LC) were Amido Black-stained membranes. Red bars indicate RB phosphorylation shift.

the SV40 large T antigen mutant (T_{121}), which specifically inactivates RB orthologs after the addition of doxycycline (Conklin et al., 2012). Upon prolonged DNA damage, RB family inactivation impaired both the cell cycle arrest and senescence onset despite high p21 levels, as shown by strong Ki67 and CycA expression (Fig. 2J; Fig. S2D,E). Collectively, these results suggest that p21 initiates G2 cell cycle exit and subsequent senescence onset by binding to and inhibiting CycD1–CDK complexes, thereby blocking RB phosphorylation after G2 arrest (Fig. S2F).

Chk1 activity drives G2 arrest but its p53-dependent downregulation associates with G2 exit

Next, we asked whether p21 is sufficient to ensure a stable G2 arrest preceding the G2 exit or if it acts in synergy with Chk1/Chk2 checkpoint kinases. The robustness of the G2/M checkpoint depends on the level of DNA damage above a certain threshold (Löbrich and Jeggo, 2007). Therefore, the maintenance of G2 arrest and its conversion to a permanent G2 exit might depend on the strength of DNA damage signalling, with higher levels translating

Journal of Cell Science (2022) 135, jcs259114. doi:10.1242/jcs.259114

into increased Chk1/Chk2 activity and/or p21 induction. To test this hypothesis, HDFs were synchronized in early S phase (favouring a G2 arrest) by release from contact inhibition and exposed to two different γ-ray doses (5 and 10 Gy) or bleomycin (24 h; Fig. S3A). Both doses upregulated p21 and induced cell cycle exit, as documented by accumulation of hypophosphorylated p130, inhibition of RB phosphorylation, downregulation of RB and CycA and stabilisation of G1 cyclins (Fig. 3A). However, whereas cells arrested predominantly in the G2 phase after exposure to 10 Gy, when exposed to 5 Gy, most cells entered mitosis and arrested in G1 (Fig. 3B; Fig. S3A). Accordingly, a robust G2 arrest correlated with initially stronger Chk1 phosphorylation (Fig. 3A, 10 Gy). In contrast, despite stronger p53 phosphorylation after exposure to 10 Gy, p21 induction and Chk2 phosphorylation were comparable between the two γ-ray doses (Fig. 3A). This suggests that the intensity and persistence of Chk1 activation, rather than p21 levels, determine whether cells will arrest and exit the cell cycle in G2, or progress into mitosis and exit in G1. If this is true, then stronger Chk1 activation should confer a more robust G2 arrest even if cells cannot induce p21. Indeed, after exposure to 10 Gy, most p53-deficient E6-expressing HDF cells (HDF-E6 cells) exhibiting elevated Chk1 phosphorylation arrested in G2, whereas after exposure to 5 Gy, they progressed into the next cell cycle as shown by fluorescence-activated cell sorting (FACS) analysis (Fig. 3C,D; Fig. S3B). These results were further corroborated by time-lapse studies showing that stronger and sustained Chk1 activation by bleomycin correlated with a robust G2 arrest, whereas HDF-E6 cells treated with ICRF-193 exhibiting more transient Chk1 phosphorylation entered mitosis despite Chk2 activation (Fig. 3E,F; Fig. S3C). Similar conclusions regarding the role of Chk1 in stabilizing the G2 arrest were previously obtained using another cellular model (Johmura et al., 2016). However, in agreement with our previous observations (Baus et al., 2003), both G1- and G2-arrested HDF-E6 cells failed to exit the cell cycle, as documented by persistent RB hyperphosphorylation and Ki67 expression (Fig. 3D; Fig. S2A,B).

Surprisingly, given its key role in stabilizing G2 arrest, Chk1 phosphorylation and protein levels decreased before the onset of cell cycle exit (24 h), contrasting with continuous Chk2 and p53 phosphorylation (Fig. 3A, lower panel). This transient nature of Chk1 phosphorylation was not specific to irradiation since it was also observed in cells exposed to bleomycin or ICRF-193 (Fig. S3C,D). In contrast, both Chk1 phosphorylation and protein levels were maintained in HDF-E6 cells arrested in G2 by radiation or bleomycin (Fig. 3D,F). Thus, sustained Chk1 phosphorylation was associated with impaired cell cycle exit. Conversely, Chk1 was strongly downregulated both in DNA damage-induced and replicative senescence (Fig. S3E,F). Taken together, these results highlight a correlation between the onset of G2 exit and suppression of Chk1, but not Chk2, signalling by the p53-p21 pathway, suggesting their differential roles in the G2-arrest-to-G2-exit conversion.

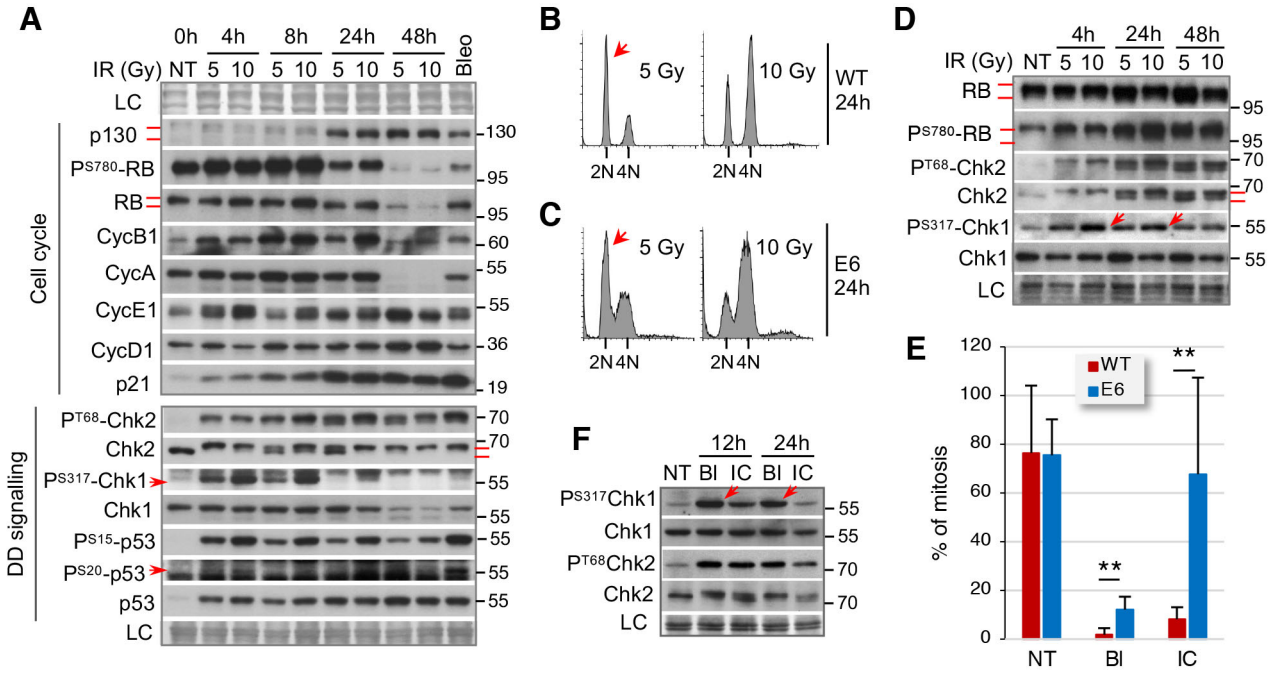

Fig. 3. Chk1 activity drives G2 arrest but its p53-dependent suppression associates with G2 exit. (A) Immunoblots of the indicated cell cycle regulators (upper panel) and DNA damage (DD) signalling effectors (lower panel) in HDFs that were exposed to ionizing radiation (IR; 5 or 10 Gy) or treated with bleomycin (Bleo) for 24 h after a release from G0 by contact inhibition (16–24 h) (n=3). FACS is shown in Fig. S3A. NT, non-treated cells (0 h time point); LC, loading control. Red bars indicate p130, RB and Chk2 phosphorylation shifts. Red arrows indicate P^{S20}-p53 and P^{S317}-Chk1 bands. (B,C) DNA content profiles by flow cytometry of wild-type (WT) (B) and HPV16-E6-expressing (E6) (C) HDFs collected after 24 h exposure to ionizing radiation (n=3). Red arrows: G1 cells. (D) Immunoblots showing persistent RB and Chk1 phosphorylation and the absence of their downregulation in HDF-E6 cells irradiated with 5 or 10 Gy doses (n=2). NT, non-treated cells; LC, loading control. Red bars indicate RB and Chk2 phosphorylation shifts. Red arrows indicate stronger P^{S317}-Chk1 signal in 10 Gy. (E) Percent of cells entering mitosis in wild-type (WT) and HPV16-E6-expressing (E6) HDFs incubated with ICRF-193 (IC) or bleomycin (BL) for 24 h. Mitosis number was scored from phase contrast images recorded by video microscopy (values are mean±s.d. of three fields from two separate experiments). **$P \leq 0.01$; two-tailed paired t-test. (F) Immunoblots showing phosphorylation of Chk1 (P^{S317}) and Chk2 (P^{T68}) in extracts from HDFs expressing HPV16-E6 treated with ICRF193 (IC) or bleomycin (BI) for the indicated times (n=2). Red arrows indicate stronger P^{S317}-Chk1 signal in bleomycin-treated cells. NT, non-treated cells; LC, loading control. Complete immunoblot analysis of WT and E6 cells is shown in Fig. S3C. In all immunoblots, loading controls (LC) were Amido Black-stained membranes.

Journal of Cell Science (2022) 135, jcs259114. doi:10.1242/jcs.259114

G2 exit associates with γH2AX downregulation and reduction of DNA damage foci

We wondered if Chk1 downregulation might be a part of the switching off of DNA damage signalling that is associated with the onset of G2 exit. To explore this possibility, we analysed the signal intensity of the DNA damage marker γH2AX by immunofluorescence and the number of DNA damage-induced foci at different times after exposure to ICRF-193, in both wild-type and E6-expressing HDFs. As predicted, G2 exit (48–72 h) correlated with a marked reduction of both the number of γH2AX and 53BP1 foci and the γH2AX signal, which were strongly attenuated by E6-expression (Fig. 4A–D). It is unlikely that the observed downregulation of the DNA damage response signalling is due to DNA damage repair (Chowdhury et al., 2005) or checkpoint recovery (Macurek et al., 2010) since the experimental conditions induced massive DNA damage, causing senescence. Moreover, reduction of the number of γH2AX and 53BP1 foci correlated with an increase in foci size (Fig. 4A,B), which might reflect their clustering associated with delayed repair. These large foci resemble 53BP1 nuclear bodies that form in the G1 phase after unrepaired DNA damage or unresolved replication stress in the preceding cycle (Lukas et al., 2011). Significantly, in addition to the absence of Chk1 phosphorylation (Fig. S3E,F), most senescent cells also exhibited low γH2AX signal and reduced numbers of larger DNA damage foci (Fig. 4E). Based on our results, we suggest that the G2 exit and mechanism of senescence onset involve downregulation of Chk1 and ATM/ATR signalling via the p53-RB pathway (Fig. 4F).

Sustained Chk1 activity in G2-arrested U2OS cells coincides with altered mitotic bypass and delayed G2 exit

If G2 exit requires Chk1 downregulation, then one might expect that prolonged Chk1 activity due to sustained DNA damage, previously observed in p53/RB-proficient cancer cell lines (Lossaint et al., 2011) or p53-deficient cells (Davoli et al., 2010), would be

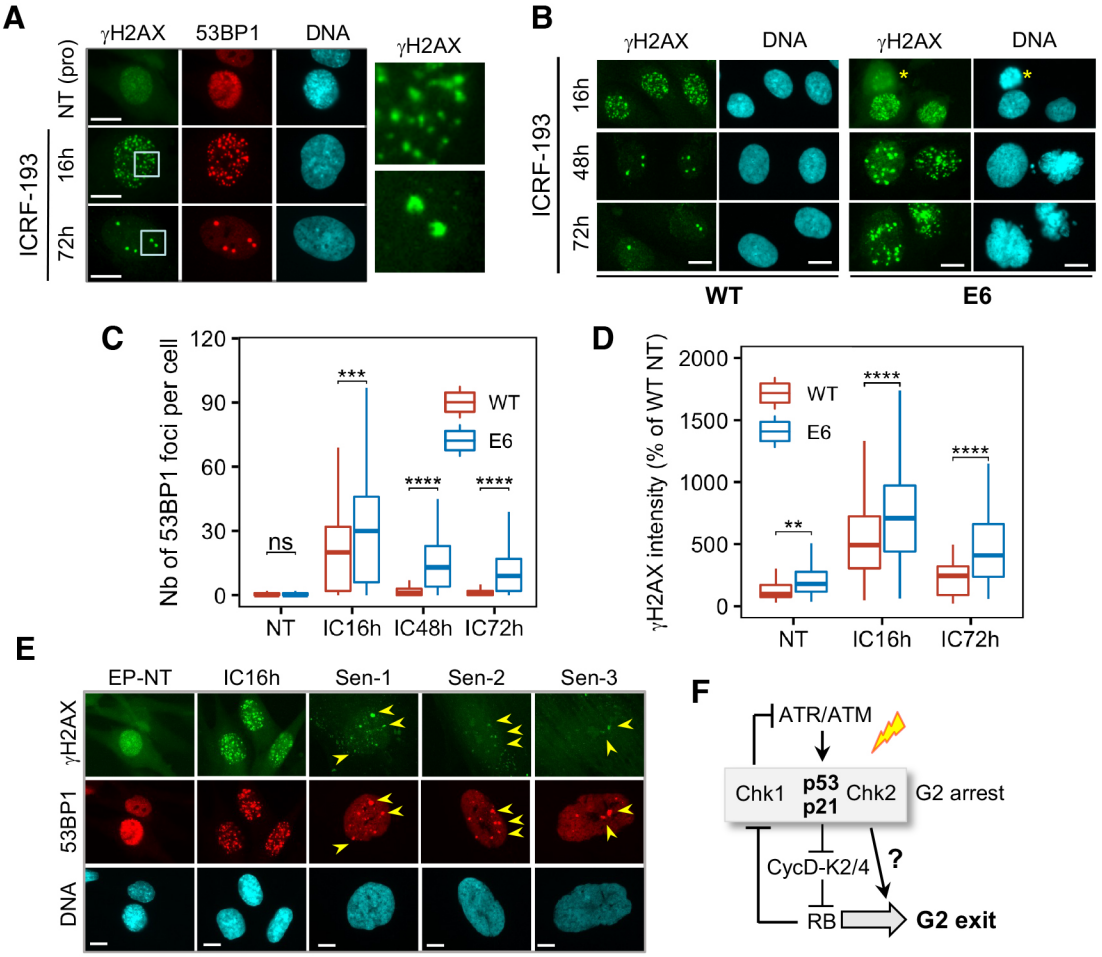

Fig. 4. G2 exit associates with γH2AX downregulation and reduction of DNA damage foci. (A) Representative immunofluorescence images (*n*=3) showing co-localization of γH2AX and 53BP1 foci in non-treated [NT, cell in prophase (pro)] HDFs and HDFs treated with ICRF-193 for the indicated times. Scale bar: 10 µm. Right panel shows magnified areas (white squares) to appreciate differences in the size/shape of γH2AX foci in cells exposed to ICRF-193 for 16 h (top) and 72 h (bottom). (B) Representative immunofluorescence images (*n*=2) showing γH2AX foci in WT and E6-expressing HDFs treated with ICRF-193 for the indicated times. The asterisk (*) denotes a cell in prophase. Scale bar: 10 µm. (C) Quantification of 53BP1 foci in WT and E6-expressing HDF cells exposed to ICRF-193 (IC) for the indicated times. NT, non-treated cells. Cells (>200) were pooled from three independent experiments. (D) Quantification of nuclear γH2AX foci intensity in WT and E6-expressing HDFs exposed to ICRF-193 for the indicated times (expressed as a percentage of γH2AX foci intensity in NT cells). Cells (>100) were pooled from three independent experiments. NT, non-treated cells. ns, not significant, $^{**}P\leq0.01$, $^{***}P\leq0.001$, $^{****}P\leq0.0001$; two-tailed unpaired *t*-test. For box plots in C,D, the box represents the 25–75th percentiles, central line indicates the median, and whiskers indicate the 10th and 90th percentiles. (E) Immunofluorescence images showing co-expression and co-localization of γH2AX and 53BP1 foci in non-treated (NT) early passage HDFs (EP-NT), HDFs treated with ICRF-193 (IC16 h) and in several representative senescent HDFs (PD 84) (*n*=3). Arrows indicate γH2AX/53BP1 foci in senescent cells. Scale bars: 10 µm. (F) Proposed roles for p53/p21 and CycD1–RB modules in suppressing Chk1 and ATM/ATR signalling during G2-arrest-G2-exit switch. K2/4, CDK2/CDK4.

Journal of Cell Science (2022) 135, jcs259114. doi:10.1242/jcs.259114

incompatible with its onset. To address this hypothesis, we studied U2OS osteosarcoma cells that, when exposed to genotoxic agents, arrest predominantly in G2 due to a deficient ATM signalling, retarded p21 induction and persistent Chk1 activation (Fig. S4A,B; Kleiblova et al., 2013; Lossaint et al., 2011). Similarly, γ-irradiation (IR) led to delayed p21 induction and sustained dose-dependent Chk1 phosphorylation, for which the intensity correlated well with the robustness of G2 arrest as documented by FACS analysis and prolonged presence of CycB1 in cells exposed to 10 Gy irradiation (Fig. 5A,B, upper panel; Fig. S4A,B).

Consistent with our hypothesis, cell cycle exit was strongly impaired in G2-arrested U2OS cells, as documented by persistent RB hyperphosphorylation and CycA expression in both irradiated cells and cells exposed to genotoxic agents (Fig. 5B, lower panel;

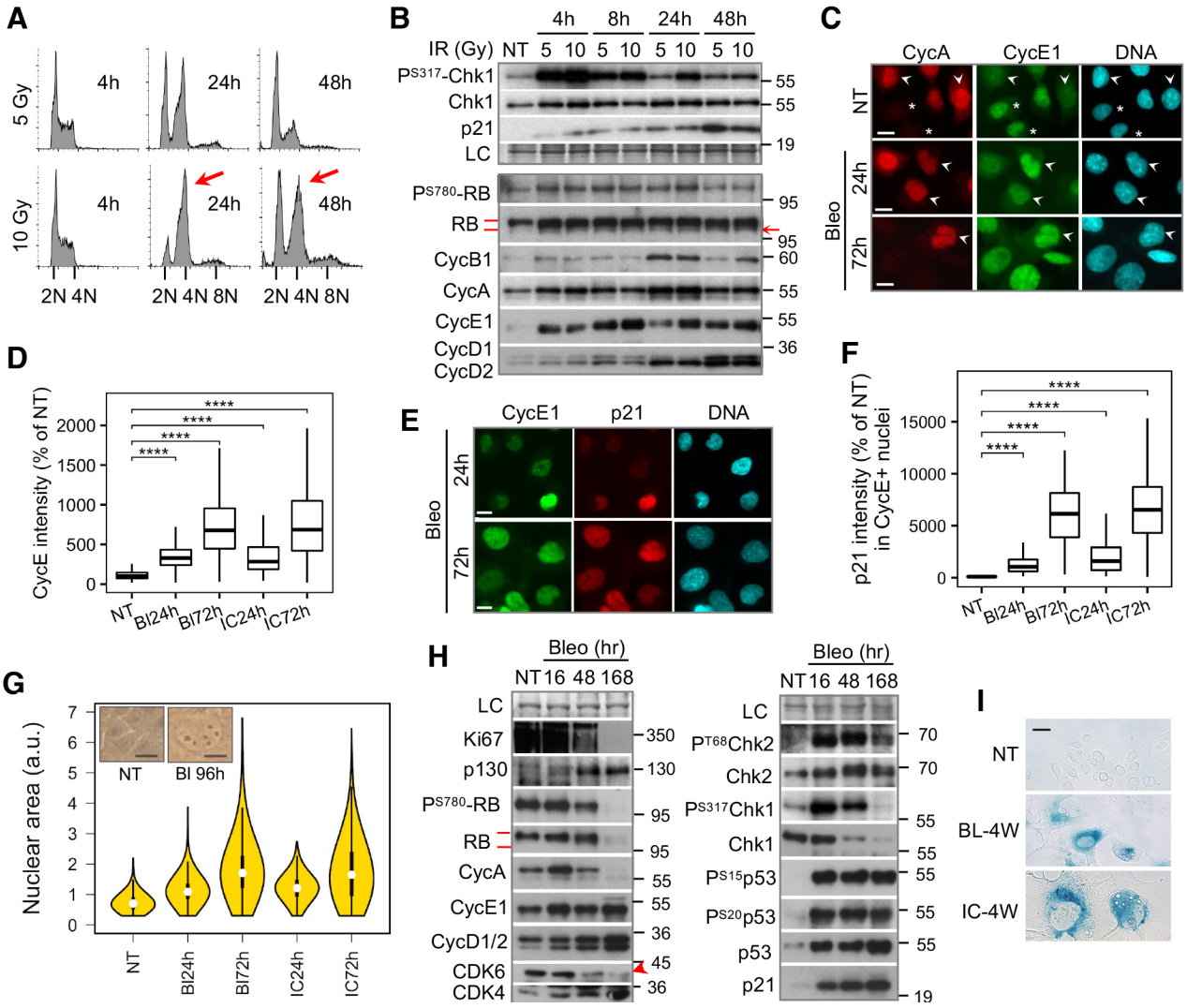

Fig. 5. Sustained Chk1 activation after G2 arrest coincides with altered mitotic bypass and delayed G2 exit in U2OS cells. (A) DNA content profiles obtained by flow cytometry of U2OS cells at the indicated times after irradiation (5 or 10 Gy) (*n*=2). Note that a more robust G2 arrest occurs in cells irradiated with 10 Gy (red arrows). (B) Immunoblots showing changes in Chk1 phosphorylation, p21 expression (upper panel) and the indicated cell cycle regulators (lower panel) in U2OS cells exposed to two doses of ionizing (γ) radiation (IR; 5 or 10 Gy) (*n*=2). NT, non-treated cells; LC, loading control. Red bars: RB phosphorylation shift; red arrow: hypophosphorylated RB. (C) Representative immunofluorescence images (*n*=2) showing CycE1/CycA co-expression in non-treated (NT) U2OS cells and cells treated with bleomycin (Bleo) for 24 or 72 h. Asterisk in NT: G1 cells lacking CycA; arrowheads: CycA-positive cells with low (NT) and high (Bleo) CycE1 expression. Scale bars: 10 µm. (D) Quantification of CycE1 intensity in U2OS cells treated with bleomycin (BL) or ICRF-193 (IC) for 24 or 72 h (expressed as a percentage of CycE1 intensity in NT). Cells (>200) were pooled from two independent experiments. NT, non-treated cells. (E) Representative immunofluorescence images (*n*=2) showing CycE1/p21 co-expression in U2OS cells treated with bleomycin (Bleo) for the indicated times. Scale bar: 10 µm. (F) Quantification of p21 intensity in CycE1-expressing U2OS cells treated with bleomycin for the indicated times (expressed as a percentage of p21 intensity in NT). Cells (>200) were pooled from two independent experiments. NT, non-treated cells. For box plots in D,F, the box represents the 25–75th percentiles, central line indicates the median, and whiskers indicate the 10th and 90th percentiles. ***$P \leq 0.0001$; two-tailed unpaired *t*-test. (G) Violin plots showing nuclear size in non-treated (NT) U2OS cells and cells exposed for 24 and 72 h to bleomycin (Bleo) or ICRF-193 (ICRF). More than 500 cells were analysed in each experiment (*n*=2). Inserts are micrographs showing NT and cells exposed for 96 h to bleomycin. a.u., arbitrary units. Scale bars: 10 µm. (H) Immunoblots showing the effects of prolonged incubation with bleomycin (Bleo) on the indicated cell cycle regulators (left panel) and DNA damage signalling effectors (right panel) in U2OS cells (*n*=2). NT, non-treated cells; LC, loading control. Arrowhead (left panel) shows CDK6 downregulation. (I) Phase contrast images showing β-galactosidase staining of U2OS cells exposed to bleomycin (BI) or ICRF-193 (IC) for 4 weeks. Scale bar: 10 µm. In all immunoblots, loading controls (LC) are Amido Black-stained membranes. Red bars: RB phosphorylation shift.

Journal of Cell Science (2022) 135, jcs259114. doi:10.1242/jcs.259114

Fig. S4C–E). In addition, immunofluorescence results showed that in bleomycin- and ICRF-193-treated cells re-accumulation of CycE1 occurred before CycA downregulation, revealing the alteration of mitotic bypass associated with DNA re-replication (Fig. 5B,C; Fig. S5A–D). However, extended G2 arrest entailed strong upregulation of D-type cyclins, which correlated with p21 induction and its increased co-expression with CycE1 (Fig. 5B–F; Fig. S4B,C, Fig. S5E–G). The concomitant decrease of CycA-positive cells and the increase of hypophosphorylated RB and p130 (Fig. 5B,C; Fig. S4C, Fig. S5A,E) indicated the onset of the G2-arrest-to-G2-exit conversion that coincided with nuclear size augmentation (Fig. 5C,E,G). Indeed, prolonged exposure to bleomycin led to a cell cycle exit in the G2 phase (Fig. S5H), documented by complete loss of Ki67 and RB phosphorylation, low RB levels, accumulation of hypophosphorylated p130 and G1 cyclins and marked CDK6 (but not CDK4) downregulation (Fig. 5H, left). Notably, G2 exit coincided with a further increase in p21 levels, concomitant with sustained p53 and Chk2 phosphorylation (Fig. 5H, right). This contrasted with a complete suppression of Chk1 phosphorylation associated with low Chk1 levels, which further highlights differences between the two Chk kinases. Moreover, G2 exit was followed by senescence, as shown by SA-β-gal staining, but this became apparent only after two-week exposure to genotoxic agents (Fig. 5I; Fig. S5I). Notably, since the INK4A locus is inactivated by methylation in U2OS cells (Park et al., 2002), these results suggest that p16 is dispensable for senescence onset.

Thus, sustained Chk1 activity in G2-arrested U2OS cells associates with delayed p21 induction and impaired cell cycle exit, whereas G2 exit and the onset of senescence correlate with downregulated Chk1, persistent Chk2 activity and strong accumulation of p21 and G1 cyclins.

Acute Chk1, but not Chk2, depletion promotes DNA damage-induced cell cycle exit by upregulating p21 and inhibiting RB kinases

The striking difference in behaviour between Chk1 and Chk2 suggested that these two kinases might play opposing roles at the onset of G2 exit. Based on our results, and those showing that Chk1 inhibits p21 expression (Beckerman et al., 2009; Hsu et al., 2019) whereas Chk2 inhibits CDK (Chen and Poon, 2008), we predicted that the Chk1 downregulation should promote DNA damage-induced cell cycle exit, whereas reduced Chk2 would delay it (Fig. 6A). To test this hypothesis, we knocked down each kinase in U2OS cells, which did not significantly affect cell proliferation (Fig. S6A), before exposure to genotoxic drugs. In agreement with previous work (Bačević et al., 2017a; Lossaint et al., 2011), Chk1 KD, but not Chk2 KD, abrogated the G2 arrest induced by bleomycin, although, based on FACS results, this effect was not clear for ICRF-193 (Fig. 6B). Further inspection by video microscopy showed that the persistence of cells with 4N DNA content upon Chk1 KD in the presence of ICRF-193 was due to accumulation of binucleate G1 cells generated after cytokinesis failure (Fig. 6C).

As predicted, Chk1 depletion potently accelerated the cell cycle exit induced by DNA damage (detectable after 16 h), as shown by downregulation of Ki67 and CycA, rapid inhibition of CycD1–CDK-dependent RB phosphorylation and accumulation of hypophosphorylated p130 and G1 cyclins (Fig. 6D; Fig. S6B). Consistent with these results, Chk1 KD upregulated p21, stimulated Chk2 phosphorylation, reduced CDK6 levels (Fig. 6D; Fig. S6B) and increased the accumulation of p21-bound CycD1–CDK2/4 and CycE1–CDK2 complexes (Fig. 6E). This suggests that Chk1 KD accelerates cell cycle exit by p21-dependent inhibition of RB family kinases as well as by CDK6 downregulation. Strikingly, Chk2 KD produced exactly the opposite effect: increased Ki67 and CycA levels and increased p130 and RB phosphorylation, and it did not upregulate G1 cyclins or induce accumulation of p21-bound CycE1 or CycD1 complexes (Fig. 6D,E; Fig. S6B). Notably, Chk2 depletion did not affect p53 phosphorylation on Ser20 (Fig. S6C) nor did it prevent DNA-dependent p21 induction (Fig. 6D), challenging its presumed role in activating p53 (Chen and Poon, 2008; Matthews et al., 2022). In agreement with these results, Chk2 KD failed to reduce p21 upregulation in HDFs treated with ICRF-193, whereas Chk1 KD strongly induced p21 and promoted cell cycle exit even in the absence of DNA damage (Fig. S6D,E). Moreover, Chk1 is not likely to compensate for the absence of Chk2 in activating p53 (Fig. S6C), since p21 induction is not reduced even upon a double Chk1/Chk2 knockdown (Fig. S6E). Thus, our results do not support a role for Chk2 in controlling p53 activity in the DNA damaged-induced G2 arrest.

Finally, we noticed a marked difference in the negative regulation of CDK4 and CDK6 in U2OS cells. Whereas both prolonged DNA damage (Fig. 5H) and Chk1 depletion (Fig. 6D) reduced CDK6, CDK4 levels increased in these situations, accumulating in p21-bound CycD1 complexes (Fig. 6E). To assess the respective contributions of CDK4 and CDK6 on RB phosphorylation, we knocked down these kinases. Although neither CDK4 KD nor CDK6 KD alone significantly affected CycD–CDK-specific RB phosphorylation, it was strongly reduced after a double CDK4/6 KD, inhibiting cell cycle progression as documented by downregulation of CDC6 and cyclin B1 (Fig. 6F). These results highlight the importance of CDK6 downregulation in DNA damage-induced cell cycle exit and senescence onset.

Taken together, our data suggest that Chk1 and Chk2 play opposing roles in the DNA damage-induced G2 exit and onset of senescence in U2OS cells (Fig. 6A). Whereas sustained Chk1 activity stabilizes G2 arrest but antagonises cell cycle exit, possibly by preventing p21-mediated inactivation of RB kinases, Chk2 might promote the latter by preventing RB phosphorylation.

Chk1 knockdown in cancer cells accelerates cell cycle exit by inducing p21 and downregulating CDK6

In U2OS cells, rapid cell cycle withdrawal induced by DNA damage and following Chk1 depletion coincided with p21 induction and CDK6 downregulation. We therefore asked whether p21 knockdown would prevent the appearance of the hallmarks of cell cycle exit in Chk1-depleted U2OS cells. To this end, we compared the effects of p21 KD, Chk1 KD and Chk1/p21 double KD (DKD) in untreated and U2OS cells exposed to bleomycin for 16 or 48 h.

Unlike Chk1 KD, p21 KD did not abrogate the G2 arrest, showing that sustained Chk1 activity can prevent mitosis even after prolonged DNA damage (Fig. 7A; Fig. S7A). In contrast, p21 depletion increased Ki67 levels and p130/RB phosphorylation, abolished G1 cyclin accumulation and supported Chk1 phosphorylation even after prolonged DNA damage (Fig. 7B; Fig. S7B). Consistent with these results, treatment with the ATM inhibitor KU-55933 (Ku), which strongly reduced p21 induction and Chk2 activation, did not abrogate G2 arrest, but it both increased CycD1-dependent RB phosphorylation and stabilised Chk1 phosphorylation (Fig. 7C; Fig. S7C). In contrast, caffeine, which inhibits both ATR and ATM, abrogated G2 arrest and reduced RB protein and phosphorylation levels (Fig. 7C; Fig. S7C). These results highlight an antagonism between Chk1 activation and ATM/p21/RB-mediated G2 exit. As

Journal of Cell Science (2022) 135, jcs259114. doi:10.1242/jcs.259114

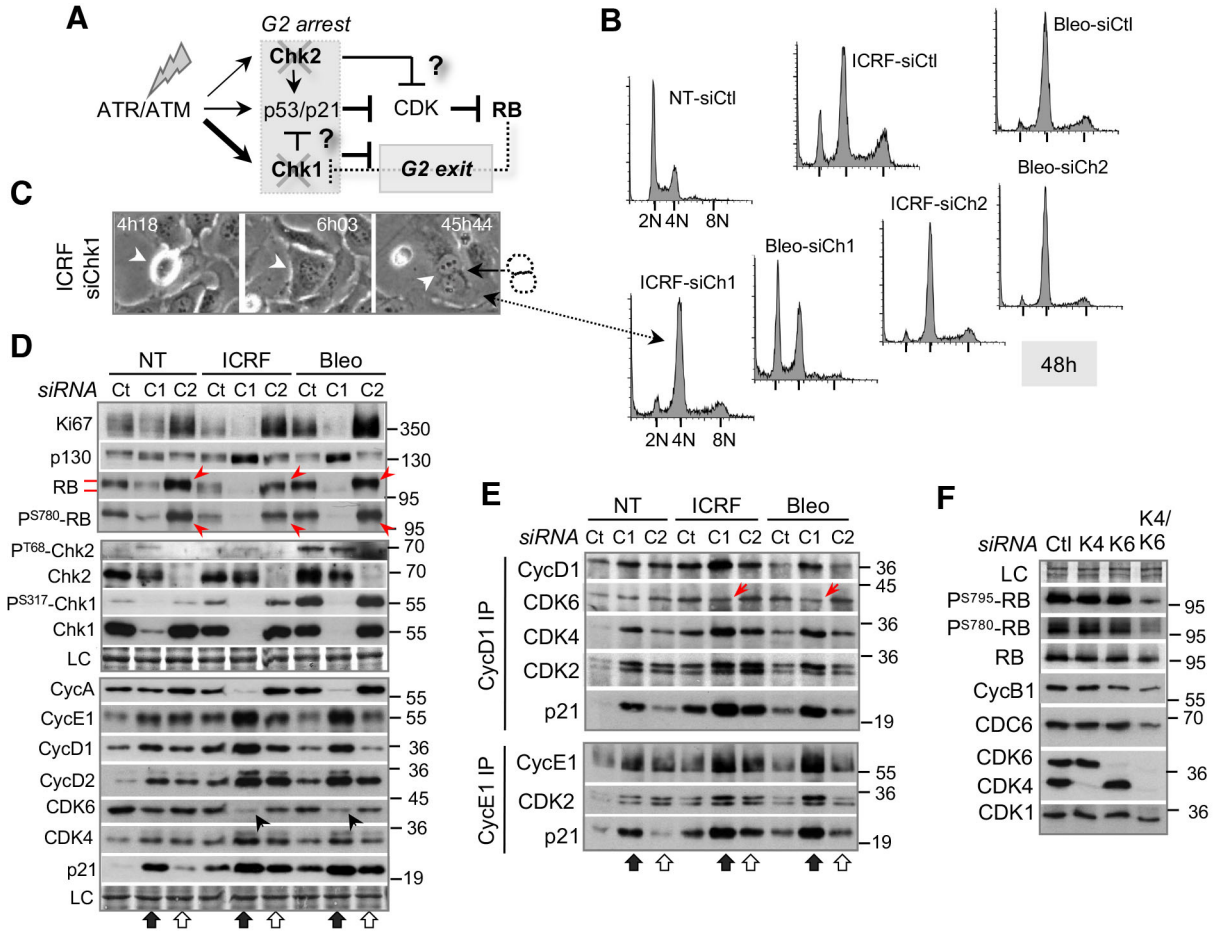

Fig. 6. Chk1, but not Chk2, depletion promotes DNA damage-induced cell cycle exit by inhibiting RB kinases. (A) Model of the expected effects of Chk1 and Chk2 knockdown on the RB pathway and DNA damage-induced G2-arrest-to-G2-exit switch. (B) DNA content profiles obtained by flow cytometry of non-treated (NT-siCtl) and siCtl, siChk1 and siChk2 U2OS cells treated with bleomycin (Bleo) and ICRF-193 (ICRF) for 48 h (*n*=2). See Fig. S6A for NT-siChk1 and NT-siChk2. siCtl, control siRNA; siCh1, Chk1 siRNA; siCh2, Chk2 siRNA. (C) Phase-contrast images from video microscopy sequences showing a binuclear daughter cell (represented by the arrow and dotted circle) after mitosis and cytokinesis failure (arrowheads) in U2OS Chk1 KD cells treated with ICRF-193 (ICRF; same condition represented in B, indicated by double-ended arrows) (*n*=2). Time after the addition of the drug is indicated. (D) Immunoblots showing the effects of Chk1 (C1, bottom black arrows) and Chk2 (C2, bottom white arrows) knockdown on Ki67 levels, RB phosphorylation and expression of the indicated cell cycle regulators in non-treated (NT) U2OS cells and cells treated with ICRF-193 (ICRF) or bleomycin (Bleo) for 48 h (*n*=2). Ct, control siRNA. LC, loading control. See Fig. S6B for the 16 h timepoint. Red bars indicate RB phosphorylation shift. Red arrows indicate increased RB phosphorylation in Chk2-depleted samples. Black arrows indicate reduction of CDK6 in Chk1-depleted samples. (E) Immunoblot analysis of cyclin D1 and cyclin E1 immunoprecipitates (IP) showing effects of Chk1 (C1, bottom black arrows) and Chk2 (C2, bottom white arrows) knockdown on cyclin–CDK–p21 complexes in U2OS cells exposed to ICRF-193 (ICRF) and bleomycin (Bleo) for 48 h (*n*=2). Red arrows: reduction of CDK6 in CycD1–CDK complexes. (F) Immunoblots showing effects of CDK4 (K4), CDK6 (K6) or double CDK4/CDK6 (K4/K6) knockdown on cyclin D1–CDK-specific RB phosphorylation (P^{S795}, P^{S780}) in U2OS cells (*n*=2). Loading controls (LC) are Amido Black-stained membranes.

predicted by our model, Chk1/p21 DKD abolished DNA damage-induced cell cycle exit (Fig. 7B), which resulted in unchecked cell cycle progression, mitotic catastrophe and, ultimately, cell death (Fig. 7A,D; Fig. S7A,D). Moreover, p21 KD counteracted Chk1 KD-mediated CDK6 downregulation (Fig. 7B, arrowheads), presumably contributing to persistent RB phosphorylation. Thus, our results confirm the key role of p21 in the onset of senescence induced by Chk1 KD in U2OS cells.

Next, we sought to validate the respective roles of Chk1 and p21 in the onset of G2 exit in another p53/RB-proficient cancer cell line, HCT-116. As with U2OS, RB phosphorylation and Ki67 levels persisted after bleomycin-induced G2 arrest and correlated with sustained Chk1 activation (Fig. 7E; Fig. S7E,F). Chk1 KD abrogated the G2 arrest and induced permanent cell cycle exit (low Ki67, unphosphorylated RB), which was associated with upregulation of p21 and G1 cyclins, strong accumulation of p21-bound CycD1–CDK2/CDK4 complexes and CDK6 downregulation (Fig. 7E,F; Fig. S7F). Conversely, while p21 KD failed to abrogate G2 arrest, it increased RB phosphorylation and prevented both CycD1/CycE1 upregulation (Fig. 7F; Fig. S7E,F) and accumulation of CycD1–CDK complexes (Fig. 7F). Furthermore, consistent with its role in mediating the Chk1 KD-induced cell cycle exit, p21 depletion fully restored Ki67, CycA and CDK6 expression, RB phosphorylation (Fig. 7E, 8 h, DKD) and abolished upregulation of CycE1 and CycD1–CDK complexes (Fig. 7F, DKD). However, after prolonged DNA damage, Chk1/p21 DKD only partially rescued Ki67 expression and RB phosphorylation in HCT-116 cells (Fig. 7E, 48 h, asterisk). The latter might be due to upregulation of the CDK inhibitor $p27^{Kip1}$ in CycD1–CDK complexes (Fig. 7F, arrow) and reduced CDK6 levels (Fig. 7E). Moreover, as in U2OS, Chk1/p21 DKD promoted cell death by abrogating checkpoints and p21-mediated senescence

Journal of Cell Science (2022) 135, jcs259114. doi:10.1242/jcs.259114

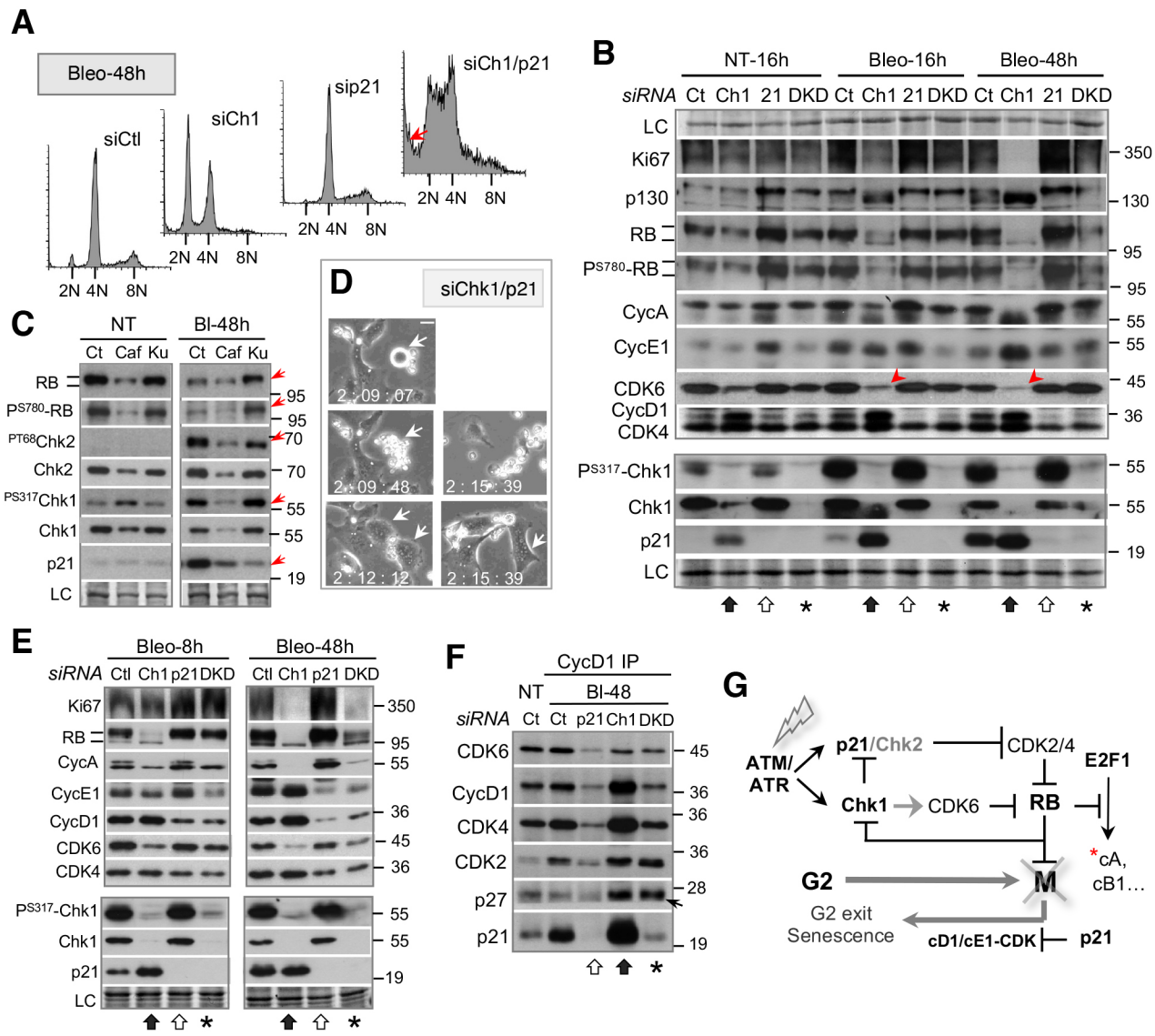

Fig. 7. Chk1 knockdown in cancer cells accelerates cell cycle exit by inducing p21 and downregulating CDK6. (A) DNA content profiles by flow cytometry of control (siCtl) and U2OS cells depleted for Chk1 (siCh1), p21 (sip21) or both (siCh1/p21) proteins treated with bleomycin (Bleo) for 48 h (*n*=2). Red arrow indicates the sub-G1 population representing dead cells. See Fig. S7A for FACS results showing effects of the respective knockdowns on non-treated U2OS cells and cells treated with bleomycin (Bleo) for 16 h. (B) Immunoblots showing the effects of Chk1 (Ch1, bottom black arrows), p21 (21, bottom white arrows) or double p21/Chk1 (DKD, asterisks) knockdown on Ki67 and the indicated cell cycle regulators (upper panel) and DNA damage signalling effectors (lower panel) in non-treated (Ctl) U2OS cells and U2OS cells treated with bleomycin (Bleo) for 16 and 48 h (*n*=2). LC, loading control. Red arrowheads indicate downregulated CDK6. (C) Immunoblots showing the effects (red arrows) of caffeine (Caf) and the ATM inhibitor KU-55933 (Ku) on RB protein and phosphorylation (P^{S780}) levels, P^{T68}-Chk2, P^{S317}-Chk1 and p21 levels in non-treated (NT) U2OS cells and cells treated with bleomycin for 48 h (*n*=2). LC, loading control. (D) Representative phase-contrast images from a video microscopy sequence showing fragmented nuclei after mitotic catastrophe in bleomycin-treated double Chk1/p21 KD cells (*n*=2). Time (days, hours, minutes) after drug addition is indicated. Arrows show a mitotic cell and the resulting daughter cells. The middle-right image shows cell debris from the same sequence. The complete field of view is shown in Fig. S7D. Scale bar: 10 µm. (E) Immunoblots showing the effects of Chk1 (Ch1, bottom black arrows), p21 (bottom white arrows) or double p21/Chk1 (DKD, asterisks) knockdown on Ki67 and the indicated cell cycle regulators in HCT-116 cells treated with bleomycin (Bleo) for 8 and 48 h (*n*=2). LC, loading control. (F) Immunoblots of CycD1 immunoprecipitates (IP) showing the effects of Chk1 (Ch1, bottom black arrow), p21 (bottom white arrow) or double p21/Chk1 (DKD, asterisk) knockdown on cyclin–CDK–CKI complexes (CKI, CDK inhibitors p21 and p27) in HCT-116 cells exposed to bleomycin (BI) for 48 h (*n*=2). In all blots, black bars on the left indicate RB phosphorylation shift, and loading controls (LC) are Amido Black-stained membranes. (G) Proposed roles for Chk1, Chk2 and p21–CycD–RB axis in DNA damage-induced senescence onset after permanent G2 arrest (G2 exit). Asterisk indicates G2/M regulators; cyclins are indicated with 'c'.

onset (Fig. S7E). Thus, p21 appears to be the main effector mediating the DNA damage-induced cell cycle exit after Chk1 depletion. In addition, our data support the role of sustained Chk1 activation in preventing p21/RB-mediated permanent G2 exit, and corroborate the importance of CDK6 downregulation in senescence onset in cancer cells.

DISCUSSION

Our results reveal that senescence onset upon the permanent DNA damage-induced G2 arrest (G2 exit) involves interplay between the p21-CycD-RB pathway and the Chk1 and Chk2 kinases (Fig. 7G). In non-transformed cells, G2 exit and senescence are triggered by p21-dependent RB activation, which correlates with Chk1

Journal of Cell Science (2022) 135, jcs259114. doi:10.1242/jcs.259114

downregulation and precedes the acquisition of senescence hallmarks such as p16 or SA-β-gal. This G2 exit programme is compromised in p53/RB-proficient cancer cells due to inefficient p21-dependent inhibition of RB phosphorylation and sustained Chk1 activation. Acute Chk1 depletion in these cells strongly accelerates cell cycle exit, in a p21-dependent manner, by inhibiting or downregulating RB kinases.

We identify CycD1–CDK2/CDK4 complexes as major p21 targets after the G2 arrest, thus uncovering their previously unrecognized role in RB phosphorylation in late cell cycle phases (Chung et al., 2019; Topacio et al., 2019). Although often considered, together with $p27^{Kip1}$, as a stabilizer, and even activator, of CycD1–CDK complexes (Sherr and Roberts, 1999), p21 was shown to inhibit CycD1–CDK4 complexes (Guiley et al., 2019; Yang et al., 2017b). Therefore, we propose that p21-CycD1 is an RB-linked DNA damage effector even beyond the G1/S transition, enabling the conversion from a temporary G2 arrest to a permanent G2 exit, which entails senescence onset (Fig. 7G). The presented results are fully consistent with our previous observations (Chassot et al., 2008) and the recent finding that CycD1 also serves as a mitogen sensor, as its elevated levels in the G2 phase of mother cells promotes daughter cell proliferation (Min et al., 2020). However, we cannot exclude the possibility that p21 triggers G2 exit by also inhibiting CycA–CDK2 which phosphorylates RB as well (Topacio et al., 2019).

In addition to its role in blocking G2/M progression, p21 targets CycD1–CDK2 and CycE1–CDK2 complexes, which accumulate upon mitotic bypass, thereby preventing re-replication (Fig. 7G) that might otherwise take place upon APC/C^{Cdh1} inactivation (Cappell et al., 2016). The importance of the inhibition of CycD1–CDK2 by p21 is highlighted by the recent discovery that this complex, which efficiently phosphorylates RB (Chytil et al., 2004; Topacio et al., 2019), might confer resistance to cancer cells against CDK4/6 inhibitors such as palbociclib (Chaikovsky et al., 2021; Saengboonmee and Sicinski, 2021). Interestingly, p21-bound CycD1/CycE1 complexes strongly accumulate in G2-arrested p53-proficient cancer cells (U2OS, HCT-116) concomitant with CycA downregulation and cell cycle exit, but their function is unclear. We speculate that these complexes, also upregulated after Chk1 depletion and previously observed in ‘spontaneously’ quiescent (Gookin et al., 2017) or senescent (Bačević et al., 2017a; Stein et al., 1999) cells, might play a role in senescence, for example, by preventing apoptosis.

The notion that p21/RB-mediated Chk1 downregulation promotes permanent cell cycle exit might appear counterintuitive, since sustained Chk1 activity stabilizes G2 arrest, in turn enabling senescence onset (Johmura et al., 2016). Nonetheless, Chk1 suppression has been observed after DNA damage-induced cell cycle arrest or in replicative senescence (Gabai et al., 2008; Gire, 2004; Gottifredi et al., 2001) and implicated in the prevention of apoptosis during trophoblast differentiation (Ullah et al., 2011). Yet, given its key role in DNA damage checkpoints, Chk1 inactivation or downregulation is often regarded as a ‘defect in the DNA damage response’ (Gabai et al., 2008), a mechanism enabling adaptation to genotoxic stress (Shaltiel et al., 2015), recovery from severe replication stress (Zhang et al., 2005) and cell cycle resumption after DNA damage repair (Park et al., 2015), or preventing a prolonged G2 arrest which might trigger apoptosis (Gottifredi et al., 2001). In contrast, our results implicate Chk1 downregulation as a necessary component of the senescence programme (Fig. 7G). The observation that telomere dysfunction in the absence of p53 associates with sustained Chk1 activation and endoreplication (Davoli et al., 2010) is fully consistent with our model. Moreover, our results suggest an explanation for the finding that an extra copy of the *CHEK1* gene promotes oncogenic transformation in mice (López-Contreras et al., 2012), which might compromise senescence onset and trigger genome instability. There are several potential mechanisms whereby prolonged Chk1 activity enables CDK-mediated RB inactivation and prevents senescence onset. For example, Chk1 might promote cell cycle progression by restraining p21 induction (Beckerman et al., 2009; Hsu et al., 2019), positively regulating CDK6 expression by inhibiting E2F6, a repressor of E2F-dependent transcription (Bertoli et al., 2013), or by phosphorylating and inactivating E2F7 and E2F8, potent transcriptional repressors (Yuan et al., 2018).

Our results showing that DNA damage-induced G2 exit correlates with p53-dependent diminution of γH2AX signal and reduction of the number of γH2AX/53BP1 foci could explain their relative low abundance observed in senescent cells (Gire et al., 2004), and could reflect an energy-saving switching off of DNA damage signalling once the cells are committed to permanent cell cycle exit. On the other hand, it is tempting to speculate that γH2AX/53BP1 foci clustering (Aymard et al., 2017), resembling 53BP1 nuclear bodies (Lukas et al., 2011), might be actively involved in senescence onset (Zhang et al., 2022).

We show that prolonged DNA damage or accelerated senescence after Chk1 depletion in cancer cells lacking p16 (Burri et al., 2001; Park et al., 2002) triggers downregulation of CDK6 but not CDK4. This finding not only underlines differential regulation of the two kinases, but also uncovers a novel, CDK inhibitor-independent mechanism of inhibiting RB phosphorylation. A nonredundant role for CDK6 in RB phosphorylation is also supported by findings in *Cdk6*$^{-/-}$ mice and our recent study where we found that CDK2 hinders cell cycle exit in part by maintaining CDK6 expression (Bačević et al., 2017a). Moreover, acquired CDK6 overexpression confers cancer resistance to CDK4/6 and CDK1/2 inhibitors (Yang et al., 2017a; Bačević et al., 2017b). Interestingly, CDK6 appears to be less targeted by p21 than CDK4 or CDK2, but upon DNA damage (this study) or in differentiation (Fujimoto et al., 2007), permanent cell cycle arrest correlates with its downregulation. And in replicative senescence, p16-mediated CDK6 sequestration preferentially downregulates CycD1–CDK6 but not CycD1–CDK4 complexes that are p21-bound (Dulić et al., 2000; Stein et al., 1999). This explains why prolonged DNA damage, which entails CDK6 downregulation, promotes senescence in U2OS cells despite the absence of p16.

Perhaps the most surprising result is that acute Chk2 depletion did not affect p53 phosphorylation or p21 induction, which would have been expected from its role as a p53 activator (Chen and Poon, 2008; Matthews et al., 2022), but instead stimulated RB phosphorylation and Ki67 expression in G2-arrested cells. While our present and earlier results (Bačević et al., 2017a; Lossaint et al., 2011) do not support its presumed but still debated role in G2 arrest (Stolz et al., 2011), they suggest that Chk2 might promote senescence by inhibiting RB kinases (Fig. 7G). This is consistent with its role in senescence (Chen and Poon, 2008; Gire et al., 2004) and as a global tumour suppressor associated with DNA damage (Stolz et al., 2011; Stracker et al., 2008).

In conclusion, our results support a model in which reciprocal regulation of p21 and Chk1 is a core feature of a network that includes both checkpoint (Chk1 and Chk2) and senescence (p21 and RB) regulators, where their combined output controls the fate of G2-arrested cells. Therefore, inhibiting Chk1 in cancers might have therapeutic benefits in combination with genotoxic chemotherapy,

as it should promote the senescence of cancer cells subjected to DNA damage. As opposed to 'synthetic lethality', we propose that 'synthetic senescence promotion' would be an appropriate description of such an effect.

MATERIALS AND METHODS

Cell lines

Normal human diploid foreskin fibroblasts (HDFs), HDFs expressing HPV16-E6 (HDF-E6 cells) and human mammary epithelial cells (HMECs) were obtained from frozen stocks, cultured and synchronized as described previously (Baus et al., 2003; Lossaint et al., 2011). U2OS (human osteosarcoma) cells were originally purchased from American Type Culture Collection (ATCC; Manassas, VA, USA) and HCT-116 (colon carcinoma) cells were a gift from Dr B. Vogelstein (Johns Hopkins University, Baltimore, MD, USA). The human fibroblasts (BJ cells) expressing the inducible SV40 mutant (T_{121}) specifically targeting pocket proteins (Conklin et al., 2012) were a gift from Dr J. Sage (Stanford, CA, USA, in 2018). Cell lines were not authenticated but were tested weekly for mycoplasma contamination (Mycolalert kit, Basel, Switzerland). Population doubling (PD) number is the total number of times the cells in a given population had doubled during *in vitro* culture. PD was calculated after each passage and the sum was taken to give the total PD.

HMECs were cultured in Mammary Epithelial Cell Growth Medium (MEGM; Lonza, Basel, Switzerland) and HCT-116 cells were cultured in McCoy's 5A medium (Gibco® Life Technologies, Waltham, MA, USA). All other cell lines were cultured in Dulbecco's Modified Eagle Medium (DMEM, high glucose, pyruvate, GlutaMAX – Gibco® Life Technologies, Waltham, MA, USA) supplemented with 10% foetal bovine serum (Sigma-Aldrich, St Louis, MO, USA; Dutcher, Bernolsheim, France; or HyClone, Cytiva, Marlborough, MA, USA). Cells were grown under standard conditions at 37°C in a humidified incubator containing 5% CO_2.

Cell drug treatments and radiation

The radiomimetic agent bleomycin (Bleomycin sulphate #S1214, Euromedex, Souffelweyersheim, France, 10 µg/ml) and the topoisomerase II inhibitor ICRF-193 [bis(2,6-dioxopiperazin), 2 µg/ml; Sigma-Aldrich, St Louis, MO, USA] were added to asynchronously growing cells as described previously (Baus et al., 2003). Where indicated, cells were irradiated (5 or 10 Gy) in the panoramic ^{60}Co γ-irradiation facility at the Ruđer Bošković Institute (Zagreb, Croatia; Majer et al., 2019). Caffeine (Sigma-Aldrich; 5 mM) and the ATM inhibitor KU-0055933 (Kudos Pharmaceuticals, Cambridge, UK; 10 µM) were added 1 h before treatment with drugs. Doxycycline (ThermoFisher, Waltham, MA, USA) was added 6–12 h before adding the genotoxic drugs (1 µg/ml).

Cell cycle analysis

Cell cycle analysis was determined by FACS of propidium iodide (PI)-stained cells using a BD FACSCalibur Flow Cytometer (BD Biosciences, San Jose, CA, USA) as described earlier (Bačević et al., 2017a). Cells were harvested, washed with cold PBS, resuspended in 300 µl PBS and fixed with 700 µl ice-cold 100% methanol. Fixed cells were kept at −20°C. For the analysis, cells were pelleted by centrifugation at 250 ***g*** for 5 min. After washing once with 1% bovine serum albumin (BSA) in PBS, cells were stained with PI staining solution (10 µg/ml PI, 1% BSA, 200 µg/ml RNase A in PBS) for 15 min at room temperature and subjected to cell cycle analysis using the BD FACSCalibur Flow Cytometer. Data were analysed using FlowJo software (v10.6.1, FlowJo, LLC, Ashland, OR, USA).

siRNA transfection

The SMARTpool ON-TARGETplus siRNAs (CHK1, CHK2, CDK2, CDK4, CDK6 or CDKN1A/p21) were purchased from GE Dharmacon Research (Lafayette, CO, USA). As control, we used siRNA for luciferase, 5′-ACUGACGACUCUGCUACUC-3′ (Luc; Eurogentec, Seraing, Belgium) or ON-TARGETplus Non-targeting siRNA #1 (Cont; GE Dharmacon). Cells were transfected with siRNA (40 nM) using a standard calcium phosphate transfection method (Bačević et al., 2017a). 24 h after transfection, the cells were exposed to genotoxic agents for the indicated times and harvested for biochemical or immunofluorescence analyses or monitored by video microscopy (Lossaint et al., 2011).

Cell lysates and samples for SDS-PAGE and immunoblotting were prepared as described previously (Baus et al., 2003; Stein et al., 1999). Briefly, cells were harvested by trypsinisation and washed in cold PBS prior to freezing in liquid nitrogen. Frozen pellets (kept at −80°C) were lysed in lysis buffer [150 mM NaCl, 50 mM Tris-HCl pH 7.5, 0.2% NP-40, 2 mM EDTA, 1 mM DTT, 0.1 mM Na_3VO_4, protease inhibitor cocktail (Sigma-Aldrich, P 8340)] and incubated on ice for 60 min. Lysates were centrifuged at 20,000 ***g*** (5 min) and the supernatant was frozen at −80°C. Total protein was quantified using the BCA Protein Assay Kit (Pierce Biotechnology; ThermoFisher, #23227). For immunoblot analysis, cell lysates were denatured in Laemmli buffer and boiled at 95°C for 5 min. 30 µg of protein was loaded into each lane. Samples were run on 7.5%, 11% or 12.5% SDS-PAGE gels, depending on the proteins of interest, and transferred to Immobilon membranes (Merck Millipore, Burlington, MA, USA) using Owl HEP-1 Semidry Electroblotter (ThermoFisher). Membranes were routinely stained with Naphthol Blue Black (Amido Black; Sigma-Aldrich, 3393) to verify the transfer and loading. Primary antibodies were diluted in 5% milk in TBS with 0.2% Tween-20 (TBS-T) and incubated for 2 h at room temperature (RT) or overnight at 4°C. Secondary antibodies (goat anti-mouse IgG-HRP, DACO, Glostrup, Denmark and donkey anti-rabbit IgG-HRP, GE Healthcare, Chicago, IL, USA) were diluted 1:5000 in 5% milk in TBS-T and incubated for 1 h at RT. Chemiluminescence was detected using Western Lightning Plus/Ultra (PerkinElmer, Villebon sur Yvette, France) and Amersham Hyperfilm™ (GE Healthcare, Chicago, IL, USA). Full immunoblot images are shown in Fig. S8.

Antibodies

The primary antibodies used for western blotting were: cyclin D1 [Santa Cruz Biotechnology (SCBT), Dallas, TX, USA; DCS-6, sc-20044], cyclin D2 (SCBT, sc-593), cyclin D3 (SCBT, sc-182), cyclin E1 (SCBT, sc-247), cyclin A (Novocastra Laboratories Ltd., Newcastle upon Tyne, UK; 6E6), cyclin B1 (SCBT, sc-752; 1:100), CDK1 [BD Transduction Laboratories (BDTL), San Jose, CA, USA; C12720], CDK2 (Abcam, Cambridge, UK; ab128167), CDK4 (SCBT, sc-260; 1:1000), CDK6 (SCBT, sc-177), p16 (BD Pharmingen, San Diego, CA, USA; 550834; 1:100), p21 [SCBT, sc-397 and Cell Signaling Technology (CST), Danvers, MA, USA; 2946, 2947], p27 (SCBT, sc-528 and BDTL, K25020), RB (BD Pharmingen, 554136; 1:200), p130 (SCBT, sc-317; 1:200), RB phospho-S780 (CST, 9307), Chk1 (SCBT, sc-8408), Chk2 (SCBT, sc-17747), Chk1 phospho-S317 (CST, 12302), Chk1 phospho-S345 (CST, 2348), Chk2 phospho-T68 (CST, 2661), Cdc25C phospho-S216 (CST, 4901), p53 (SCBT, sc-126), p53 phospho-S15 (CST, 9284), Ki67 (Abcam, ab16667) and CDC6 (SCBT, sc-9964). Dilutions were 1:500–1:1000 for antibodies against total proteins or 1:100–1:200 for antibodies against phosphorylated proteins, unless otherwise specified. For more details on the antibodies, see Table S1.

Co-immunoprecipitation and p21 immuno-depletion

Cells were lysed as described above. Routinely, 100–200 µg of total cell protein was used per immunoprecipitation (IP) and antibodies against target proteins were added at a concentration of 4 µg antibody/mg of total protein, unless otherwise specified. Samples were incubated with the primary antibody for 2 h at 4°C and the immunocomplexes were recovered using Protein A or Protein G Sepharose beads (Amersham Biosciences, Piscataway, NJ, USA; 10 µl beads/100 µl of lysates). Beads were washed in TBS-T, and immunoprecipitated proteins were eluted in 2× Laemmli buffer by heating at 37°C for 15 min. To detect proteins on immunoblots containing immunoprecipitates, peroxidase-conjugated protein A/G was used (Pierce Biotechnology, Rockford, IL, USA; 32490). The primary antibodies used for immunoprecipitations were: cyclin E1 (SCBT, sc-248), p21 (SCBT, sc-397), p27 (SCBT, sc-528) and rabbit polyclonal anti-cyclin D1 (Dulić et al., 1993; 1 µl/100 µl of lysate). For more details on the antibodies, see Table S1.

For p21 or p27 immuno-depletion experiments, cell lysates (100–200 µg) were incubated with saturating amounts of p21 or p27 antibodies, whereas mock samples were incubated with protein A–Sepharose only. The resulting

supernatants were analysed by immunoblotting as described previously (Stein et al., 1999). Full immunoblot images are shown in Fig. S8.

Immunofluorescence and image analysis

The experimental conditions for immunofluorescence, primary antibodies used and methods for image acquisition and analysis have been published previously (Bačević et al., 2017a; Lossaint et al., 2011). Briefly, cells were seeded on coverslips and fixed in cold 100% methanol (10 min, −20°C) or formaldehyde (3.7%, 15 min, RT). Prior to incubation with primary antibodies (1–2 h at RT in a humidified chamber) formaldehyde-fixed cells were permeabilized in PBS with 0.2% Triton X-100. Primary and secondary antibodies were diluted in blocking solution [0.1% Tween-20 in PBS with 5% fetal calf serum (FCS; Sigma-Aldrich; Dutcher, Bernolsheim, France; or HyClone, Cytiva, Marlborough, MA, USA), 2 h, RT]. After washing in PBS with 0.1% Tween-20 (three times for 5 min), the cells were incubated with secondary antibody (1 h at RT) and washed again (three times for 5 min). Secondary antibodies were diluted 1:1000 for the fluorophores Alexa Fluor 488, Alexa Fluor 555 and Alexa Fluor 568, and 1:500 for Alexa Fluor 647 (Invitrogen, Fisher Scientific). Coverslips were rinsed in distilled water prior to mounting on slides with ProLong Diamond Antifade Mountant with DAPI (Molecular Probes, Eugene, OR, USA, P36962). Immunofluorescence images were captured on a Leica CTR6000 microscope (objective, Leica 40× HCX PL APO 1.25-0.75 oil; camera, CollSnap HQ2; Wetzlar, Germany) driven by MetaMorph (MDS, Analytical Technologies, Canada). Composites were generated using Adobe Photoshop (Adobe Systems, Inc, San Jose, CA, USA) and Microsoft PowerPoint (Microsoft Corp, Redmond, WA, USA). For the panels showing immunofluorescence images, a representative field was shown.

The following primary antibodies were used: cyclin E1 (HE12, SCBT, sc-247; 1:100), cyclin D1 (CST, 2926; Abcam, ab16663), cyclin A (Novocastra, 6E6 and SCBT, sc751), cyclin B1 (SCBT, sc-752; 1:100), p21 (CST, 2946, 2947), H2AX phospho-S139 (Merck Millipore, clone JBW301, 05-636), 53BP1 (Novus Biologicals, Littleton, CO, USA; NB100-304) and Ki67 (Abcam, ab16667 and BDTL, 610968). Dilutions were 1:500 unless otherwise specified. For more details on the antibodies, see Table S1.

Every experiment was performed at least twice with each genotoxic agent. For each condition, at least ten images (40× magnification) were taken with a widefield fluorescent microscope for each situation. Immunofluorescence signals were quantified using a custom script in ImageJ software (Virginie Georget, Montpellier Ressources Imagerie) as described previously (Bačević et al., 2017a). DAPI images were used to identify the individual nuclei using a background correction, a mask creation based on threshold, watershed segmentation and the 'analyse particles' function in ImageJ. The region-of-interest selections corresponding to the nuclei were applied to the different channels and the total intensity of individual nuclei was quantified. The boxplots from quantification data were generated with R (version 3.6.2) and represent cell pools of at least two independent experiments. For the panels showing immunofluorescence images, representative fields were shown.

Video microscopy

Conditions for video microscopy were described previously (Bačević et al., 2017a; Lossaint et al., 2011). Mitoses were scored by inspection of video microscopy sequences (MetaMorph software). Images were taken at 10–15 min intervals for at least 48 h. Three fields for each situation were analysed and normalized for the cell number at the beginning of the time-lapse sequence. For mitosis-entry kinetics, the total number of mitotic cells during the given interval was plotted. For each experiment, all the conditions were tested in parallel, including controls with untreated cells that were transfected with different siRNAs.

SA-β-galactosidase

Conditions for SA-β-galactosidase staining using the Senescence Detection Kit (Abcam, ab655351) were described previously (Bačević et al., 2017a; Sobecki et al., 2017). HDF or U2OS cells were seeded on coverslips in 12-well plates, at a density of 10^5 cells per well. After 24 h, cells were treated with ICRF-193 (2 µg/ml) or bleomycin (10 µg/ml). The drugs were washed away from the cells after 48 h incubation, followed by staining after 2 or 4 weeks using the Senescence Detection Kit. Photos were taken using an upright microscope at 20× magnification.

Statistical analysis

Each experiment was performed independently two to three times. Data are presented as the mean±standard deviation (s.d.) or standard error of mean (s.e.m.). The two-tailed unpaired Student's *t*-test was performed using Microsoft® Excel® 2016 (Microsoft Corp, Redmond, WA, USA) to analyse the differences between the means of groups. Differences were considered statistically significant for a *P*-value of ≤ 0.05 labelled by an asterisk (*). Immunofluorescent images were quantified using ImageJ software. Box plots and violin plots were generated using R software. For all analyses, the cells were pooled from two to three independent experiments and at least 200 cells were analysed.

Acknowledgements

We are grateful to KUDOS Pharmaceuticals for the gift of KU-55933 and Dr Julien Sage (Stanford, USA) for the generous gift of T_{121}-expressing fibroblasts. We thank Dr Annick Péléraux for statistical analysis of immunofluorescence images and the figures using R software. We thank Drs Etienne Schwob, Alain Camasses, Jacques Piette, Julien Sage and Philippe Coulombe for critically reading various versions of the manuscript. Finally, we would like to thank all the reviewers, whose insightful criticisms and suggestions greatly shaped this article. We acknowledge the imaging facility Montpellier Ressources Imagerie (MRI), a member of the national infrastructure France-BioImaging, supported by the French National Research Agency (ANR-10-INBS-04, 'Investments for the Future').

Competing interests

The authors declare no competing or financial interests.

Author contributions

Conceptualization: A.H., V.D.; Software: V. Georget; Validation: V.D.; Formal analysis: V. Georget; Investigation: G.L., A.H., V. Gire, K.B., K.M., F.C.-S., V.D.; Writing - original draft: A.H., D.F., V.D.; Supervision: V.D.; Funding acquisition: D.F.

Funding

This work was supported by Fondation ARC pour la Recherche sur le Cancer (N° 3793 to V.D.) and the Cancéropôle Grand Sud-Ouest. The team (G.L., K.B., V.D., K.M. and D.F.) is 'Equipe labellisé' by the Ligue Contre le Cancer (LNCC, EL2013.LNCC/DF). G.L. and K.B. were recipients of a PhD fellowship from LNCC. A.H. was funded by Hrvatska Zaklada za Znanost (Croatian Science Foundation, grant IP-2013-11-1615). V. Gire was funded by Institut National Du Cancer (INCA, 2017-169).

Peer review history

The peer review history is available online at https://journals.biologists.com/jcs/article-lookup/doi/10.1242/jcs.259114.

References

Alcorta, D. A., Xiong, Y., Phelps, D., Hannon, G., Beach, D. and Barrett, J. C. (1996). Involvement of the cyclin-dependent kinase inhibitor p16 (INK4a) in replicative senescence of normal human fibroblasts. *Proc. Natl. Acad. Sci. USA* **93**, 13742-13747. doi:10.1073/pnas.93.24.13742

Aymard, F., Aguirrebengoa, M., Guillou, E., Javierre, B. M., Bugler, B., Arnould, C., Rocher, V., Iacovoni, J. S., Biernacka, A., Skrzypczak, M. et al. (2017). Genome-wide mapping of long-range contacts unveils clustering of DNA double-strand breaks at damaged active genes. *Nat. Struct. Mol. Biol.* **24**, 353-361. doi:10.1038/nsmb.3387

Bačević, K., Lossaint, G., Achour, T. N., Georget, V., Fisher, D. and Dulić, V. (2017a). Cdk2 strengthens the intra-S checkpoint and counteracts cell cycle exit induced by DNA damage. *Sci. Rep.* **7**, 13429. doi:10.1038/s41598-017-12868-5

Bacevic, K., Noble, R., Soffar, A., Wael Ammar, O., Boszonyik, B., Prieto, S., Vincent, C., Hochberg, M. E., Krasinska, L. and Fisher, D. (2017b). Spatial competition constrains resistance to targeted cancer therapy. *Nat. Commun.* **8**, 1995. doi:10.1038/s41467-017-01516-1

Baus, F., Gire, V., Fisher, D., Piette, J. and Dulic, V. (2003). Permanent cell cycle exit in G2 phase after DNA damage in normal human fibroblasts. *EMBO J.* **22**, 3992-4002. doi:10.1093/emboj/cdg387

Beckerman, R., Donner, A. J., Mattia, M., Peart, M. J., Manley, J. L., Espinosa, J. M. and Prives, C. (2009). A role for Chk1 in blocking transcriptional elongation of p21 RNA during the S-phase checkpoint. *Genes Dev.* **23**, 1364-1377. doi:10.1101/gad.1795709

Bertoli, C., Klier, S., McGowan, C., Wittenberg, C. and de Bruin, R. A. M. (2013). Chk1 inhibits E2F6 repressor function in response to replication stress to maintain cell-cycle transcription. *Curr. Biol.* **23**, 1629-1637. doi:10.1016/j.cub.2013.06.063

Broude, E. V., Swift, M. E., Vivo, C., Chang, B.-D., Davis, B. M., Kalurupalle, S., Blagosklonny, M. V. and Roninson, I. B. (2007). p21(Waf1/Cip1/Sdi1) mediates retinoblastoma protein degradation. *Oncogene* **26**, 6954-6958. doi:10.1038/sj.onc.1210516

Bunz, F., Dutriaux, A., Lengauer, C., Waldman, T., Zhou, S., Brown, J. P., Sedivy, J. M., Kinzler, K. W. and Vogelstein, B. (1998). Requirement for p53 and p21 to sustain G2 arrest after DNA damage. *Science* **282**, 1497-1501. doi:10.1126/science.282.5393.1497

Burri, N., Shaw, P., Bouzourene, H., Sordat, I., Sordat, B., Gillet, M., Schorderet, D., Bosman, F. T. and Chaubert, P. (2001). Methylation silencing and mutations of the p14ARF and p16INK4a genes in colon cancer. *Lab. Invest.* **81**, 217-229. doi:10.1038/labinvest.3780230

Cappell, S. D., Chung, M., Jaimovich, A., Spencer, S. L. and Meyer, T. (2016). Irreversible APC(Cdh1) inactivation underlies the point of no return for cell-cycle entry. *Cell* **166**, 167-180. doi:10.1016/j.cell.2016.05.077

Chaikovsky, A. C., Li, C., Jeng, E. E., Loebell, S., Lee, M. C., Murray, C. W., Cheng, R., Demeter, J., Swaney, D. L., Chen, S.-H. et al. (2021). The AMBRA1 E3 ligase adaptor regulates the stability of cyclin D. *Nature* **592**, 794-798. doi:10.1038/s41586-021-03474-7

Charrier-Savournin, F. B., Château, M.-T., Gire, V., Sedivy, J., Piette, J. and Dulić, V. (2004). p21-Mediated nuclear retention of cyclin B1-Cdk1 in response to genotoxic stress. *Mol. Biol. Cell* **15**, 3965-3976. doi:10.1091/mbc.e03-12-0871

Chassot, A.-A., Lossaint, G., Turchi, L., Meneguzzi, G., Fisher, D., Ponzio, G. and Dulic, V. (2008). Confluence-induced cell cycle exit involves pre-mitotic CDK inhibition by p27(Kip1) and cyclin D1 downregulation. *Cell Cycle* **7**, 2038-2046. doi:10.4161/cc.7.13.6233

Chen, Y. and Poon, R. Y. (2008). The multiple checkpoint functions of CHK1 and CHK2 in maintenance of genome stability. *Front. Biosci.* **13**, 5016-5029.

Chen, J.-Y., Lin, J.-R., Tsai, F.-C. and Meyer, T. (2013). Dosage of Dyrk1a shifts cells within a p21-cyclin D1 signaling map to control the decision to enter the cell cycle. *Mol. Cell* **52**, 87-100. doi:10.1016/j.molcel.2013.09.009

Chicas, A., Wang, X., Zhang, C., McCurrach, M., Zhao, Z., Mert, O., Dickins, R. A., Narita, M., Zhang, M. and Lowe, S. W. (2010). Dissecting the unique role of the retinoblastoma tumor suppressor during cellular senescence. *Cancer Cell* **17**, 376-387. doi:10.1016/j.ccr.2010.01.023

Chowdhury, D., Keogh, M.-C., Ishii, H., Peterson, C. L., Buratowski, C. and Lieberman, J. (2005). gamma-H2AX dephosphorylation by protein phosphatase 2A facilitates DNA double-strand break repair. *Mol. Cell* **20**, 801-809. doi:10.1016/j.molcel.2005.10.003

Chung, M., Liu, C., Yang, H. W., Koberlin, M. S., Cappell, S. D. and Meyer, T. (2019). Transient hysteresis in CDK4/6 activity underlies passage of the restriction point in G1. *Mol. Cell* **76**, 562-573.e4. doi:10.1016/j.molcel.2019.08.020

Chytil, A., Waltner-Law, M., West, R., Friedman, D., Aakre, M., Barker, D. and Law, B. (2004). Construction of a cyclin D1-Cdk2 fusion protein to model the biological functions of cyclin D1-Cdk2 complexes. *J. Biol. Chem.* **279**, 47688-47698. doi:10.1074/jbc.M405938200

Conklin, J. F., Baker, J. and Sage, J. (2012). The RB family is required for the self-renewal and survival of human embryonic stem cells. *Nat. Commun.* **3**, 1244. doi:10.1038/ncomms2254

Davoli, T. and de Lange, T. (2012). Telomere-driven tetraploidization occurs in human cells undergoing crisis and promotes transformation of mouse cells. *Cancer Cell* **21**, 765-776. doi:10.1016/j.ccr.2012.03.044

Davoli, T., Denchi, E. L. and de Lange, T. (2010). Persistent telomere damage induces bypass of mitosis and tetraploidy. *Cell* **141**, 81-93. doi:10.1016/j.cell.2010.01.031

Di Micco, R., Krizhanovsky, V., Baker, D. and Fagagna, F. d. A. d. (2021). Cellular senescence in ageing: from mechanisms to therapeutic opportunities. *Nat. Rev. Mol. Cell Biol.* **22**, 75-95. doi:10.1038/s41580-020-00314-w

Dulić, V., Drullinger, L. F., Lees, E., Reed, S. I. and Stein, G. H. (1993). Altered regulation of G1 cyclins in senescent human diploid fibroblasts: accumulation of inactive cyclin E-Cdk2 and cyclin D1-Cdk2 complexes. *Proc. Natl. Acad. Sci. USA* **90**, 11034-11038. doi:10.1073/pnas.90.23.11034

Dulić, V., Beney, G.-E., Frebourg, G., Drullinger, L. F. and Stein, G. H. (2000). Uncoupling between phenotypic senescence and cell cycle arrest in aging p21-deficient fibroblasts. *Mol. Cell. Biol.* **20**, 6741-6754. doi:10.1128/MCB.20.18.6741-6754.2000

Feringa, F. M., Raaijmakers, J. A., Hadders, M. A., Vaarting, C., Macurek, L., Heitink, L., Krenning, L. and Medema, R. H. (2018). Persistent repair intermediates induce senescence. *Nat. Commun.* **9**, 3923. doi:10.1038/s41467-018-06308-9

Fujimoto, T., Anderson, K., Jacobsen, S. E. W., Nishikawa, S.-I. and Nerlov, C. (2007). Cdk6 blocks myeloid differentiation by interfering with Runx1 DNA binding and Runx1-C/EBPα interaction. *EMBO J.* **26**, 2361-2370. doi:10.1038/sj.emboj.7601675

Gabai, V. L., O'Callaghan-Sunol, C., Meng, L., Sherman, M. Y. and Yaglom, J. (2008). Triggering senescence programs suppresses Chk1 kinase and sensitizes cells to genotoxic stresses. *Cancer Res.* **68**, 1834-1842. doi:10.1158/0008-5472.CAN-07-5656

Geng, Y., Yu, Q., Sicinska, E., Das, M., Bronson, R. T. and Sicinski, P. (2001). Deletion of the p27Kip1 gene restores normal development in cyclin D1-deficient mice. *Proc. Natl. Acad. Sci. USA* **98**, 94-99. doi:10.1073/pnas.98.1.194

Gire, V. (2004). Dysfunctional telomeres at senescence signal cell cycle arrest via Chk2. *Cell Cycle* **3**, 1217-1220. doi:10.4161/cc.3.10.1167

Gire, V. and Dulić, V. (2015). Senescence from G2 arrest, revisited. *Cell Cycle* **14**, 297-304. doi:10.1080/15384101.2014.1000134

Gire, V., Roux, P., Wynford-Thomas, D., Brondello, J.-M. and Dulic, V. (2004). DNA damage checkpoint kinase Chk2 triggers replicative senescence. *EMBO J.* **23**, 2554-2563. doi:10.1038/sj.emboj.7600259

Gookin, S., Min, M., Phadke, H., Chung, M., Moser, J., Miller, I., Carter, D. and Spencer, S. L. (2017). A map of protein dynamics during cell-cycle progression and cell-cycle exit. *PLoS Biol.* **15**, e2003268. doi:10.1371/journal.pbio.2003268

Gottifredi, V., Karni-Schmidt, O., Shieh, S.-Y. and Prives, C. (2001). p53 down-regulates CHK1 through p21 and the retinoblastoma protein. *Mol. Cell. Biol.* **21**, 1066-1076. doi:10.1128/MCB.21.4.1066-1076.2001

Guiley, K. Z., Stevenson, J. W., Lou, K., Barkovich, K. J., Kumarasamy, V., Wijeratne, T. U., Bunch, K. L., Tripathi, S., Knudsen, E. S., Witkiewicz, A. K. et al. (2019). p27 allosterically activates cyclin-dependent kinase 4 and antagonizes palbociclib inhibition. *Science* **366**, eaaw2106. doi:10.1126/science.aaw2106

He, S. and Sharpless, N. E. (2017). Senescence in health and disease. *Cell* **169**, 1000-1011. doi:10.1016/j.cell.2017.05.015

Herbig, U., Jobling, W. A., Chen, B. P. C., Chen, D. J. and Sedivy, J. M. (2004). Telomere shortening triggers senescence of human cells through a pathway involving ATM, p53, and p21(CIP1), but not p16(INK4a). *Mol. Cell* **14**, 501-513. doi:10.1016/S1097-2765(04)00256-4

Hitomi, M. and Stacey, D. W. (1999). Cyclin D1 production in cycling cells depends on Ras in a cell-cycle-specific manner. *Curr. Biol.* **9**, 1075-1084. doi:10.1016/S0960-9822(99)80476-X

Hsu, C.-H., Altschuler, S. J. and Wu, L. F. (2019). Patterns of early p21 dynamics determine proliferation-senescence cell fate after chemotherapy. *Cell* **178**, 361-371. doi:10.1016/j.cell.2019.05.041

Ito, T., Teo, Y. V., Evans, S. A., Neretti, N. and Sedivy, J. M. (2018). Regulation of cellular senescence by polycomb chromatin modifiers through distinct DNA damage- and histone methylation-dependent pathways. *Cell Rep.* **22**, 3480-3492. doi:10.1016/j.celrep.2018.03.002

Jackson, M. W., Agarwal, M. K., Yang, J., Bruss, P., Uchiumi, T., Agarwal, M. L., Stark, G. R. and Taylor, W. R. (2005). p130/p107/p105Rb-dependent transcriptional repression during DNA-damage-induced cell-cycle exit at G2. *J. Cell Sci.* **118**, 1821-1832. doi:10.1242/jcs.02307

Johmura, Y., Shimada, M., Misaki, T., Naiki-Ito, A., Miyoshi, H., Motoyama, N., Ohtani, N., Hara, E., Nakamura, M., Morita, A. et al. (2014). Necessary and sufficient role for a mitosis skip in senescence induction. *Mol. Cell* **55**, 73-84. doi:10.1016/j.molcel.2014.05.003

Johmura, Y., Yamashita, E., Shimada, M., Nakanishi, K. and Nakanishi, M. (2016). Defective DNA repair increases susceptibility to senescence through extension of Chk1-mediated G2 checkpoint activation. *Sci. Rep.* **6**, 31194. doi:10.1038/srep31194

Kitagawa, M., Higashi, H., Jung, H. K., Suzuki-Takahashi, I., Ikeda, M., Tamai, K., Kato, J., Segawa, K., Yoshida, E., Nishimura, S. et al. (1996). The consensus motif for phosphorylation by cyclin D1-Cdk4 is different from that for phosphorylation by cyclin A/E-Cdk2. *EMBO J.* **15**, 7060-7069. doi:10.1002/j.1460-2075.1996.tb01097.x

Kleiblova, P., Shaltiel, I. A., Benada, J., Sevcik, J., Pecháčková, S., Pohlreich, P., Voest, E. E., Dundr, P., Bartek, J., Kleibl, Z. et al. (2013). Gain-of-function mutations of PPM1D/Wip1 impair the p53-dependent G1 checkpoint. *J. Cell Biol.* **201**, 511-521. doi:10.1083/jcb.201210031

Krenning, L., Feringa, F. M., Shaltiel, I. A., van den Berg, J. and Medema, R. H. (2014). Transient activation of p53 in G2 phase is sufficient to induce senescence. *Mol. Cell* **55**, 59-72. doi:10.1016/j.molcel.2014.05.007

Lemmens, B. and Lindqvist, A. (2019). DNA replication and mitotic entry: a brake model for cell cycle progression. *J. Cell Biol.* **218**, 3892-3902. doi:10.1083/jcb.201909032

Löbrich, M. and Jeggo, P. A. (2007). The impact of a negligent G2/M checkpoint on genomic instability and cancer induction. *Nat. Rev. Cancer* **7**, 861-869. doi:10.1038/nrc2248

López-Contreras, A. J., Gutierrez-Martinez, P., Specks, J., Rodrigo-Perez, S. and Fernandez-Capetillo, O. (2012). An extra allele of Chk1 limits oncogene-induced replicative stress and promotes transformation. *J. Exp. Med.* **209**, 455-461. doi:10.1084/jem.20112147

Lossaint, G., Besnard, E., Fisher, D., Piette, J. and Dulić, V. (2011). Chk1 is dispensable for G2 arrest in response to sustained DNA damage when the ATM/p53/p21 pathway is functional. *Oncogene* **30**, 4261-4274. doi:10.1038/onc.2011.135

Lukas, C., Savic, V., Bekker-Jensen, S., Doil, C., Neumann, B., Pedersen, R. S., Grofte, M., Chan, K. L., Hickson, I. D., Bartek, J. et al. (2011). 53BP1 nuclear bodies form around DNA lesions generated by mitotic transmission of

chromosomes under replication stress. *Nat. Cell Biol.* **13**, 243-253. doi:10.1038/ncb2201

Lundberg, A. S. and Weinberg, R. A. (1998). Functional inactivation of the retinoblastoma protein requires sequential modification by at least two distinct cyclin-cdk complexes. *Mol. Cell. Biol.* **18**, 753-761. doi:10.1128/MCB.18.2.753

Macurek, L., Lindqvist, A., Voets, O., Kool, J., Vos, H. R. and Medema, R. H. (2010). Wip1 phosphatase is associated with chromatin and dephosphorylates gammaH2AX to promote checkpoint inhibition. *Oncogene* **29**, 2281-2291. doi:10.1038/onc.2009.501

Majer, M., Roguljić, M., Knežević, Ž., Starodumov, A., Ferenček, D., Brigljević, V. and Mihaljević, B. (2019). Dose mapping of the panoramic 60Co gamma irradiation facility at the Ruđer Bošković Institute – Geant4 simulation and measurements. *Appl. Radiat. Isot.* **154**, 108824. doi:10.1016/j.apradiso.2019.108824

Matsushime, H., Quelle, D. E., Shurtleff, S. A., Shibuya, M., Sherr, C. J. and Kato, J. Y. (1994). D-type cyclin-dependent kinase activity in mammalian cells. *Mol. Cell. Biol.* **14**, 2066-2076. doi:10.1128/mcb.14.3.2066-2076.1994

Matthews, H. K., Bertoli, C. and de Bruin, R. A. M. (2022). Cell cycle control in cancer. *Nat. Rev. Mol. Cell Biol.* **23**, 74-88. doi:10.1038/s41580-021-00404-3

Min, M., Rong, Y., Tian, C. and Spencer, S. L. (2020). Temporal integration of mitogen history in mother cells controls proliferation of daughter cells. *Science* **368**, 1261-1265. doi:10.1126/science.aay8241

Park, Y.-B., Park, M. J., Kimura, K., Shimizu, K., Lee, S. H. and Yokota, J. (2002). Alterations in the INK4a/ARF locus and their effects on the growth of human osteosarcoma cell lines. *Cancer Genet. Cytogenet.* **133**, 105-111. doi:10.1016/S0165-4608(01)00575-1

Park, C., Suh, Y. and Cuervo, A. M. (2015). Regulated degradation of Chk1 by chaperone-mediated autophagy in response to DNA damage. *Nat. Commun.* **6**, 6823. doi:10.1038/ncomms7823

Roger, L., Tomas, F. and Gire, V. (2021). Mechanisms and regulation of cellular senescence. *Int. J. Mol. Sci.* **22**, 13173. doi:10.3390/ijms222313173

Sadasivam, S. and DeCaprio, J. A. (2013). The DREAM complex: master coordinator of cell cycle-dependent gene expression. *Nat. Rev. Cancer* **13**, 585-595. doi:10.1038/nrc3556

Saengboonmee, C. and Sicinski, P. (2021). The path to destruction for D-type cyclin proteins. *Nature* **592**, 690-691. doi:10.1038/d41586-021-00889-0

Shaltiel, I. A., Krenning, L., Bruinsma, W. and Medema, R. H. (2015). The same, only different - DNA damage checkpoints and their reversal throughout the cell cycle. *J. Cell Sci.* **128**, 607-620. doi:10.1242/jcs.163766

Sharpless, N. E. and Sherr, C. J. (2015). Forging a signature of in vivo senescence. *Nat. Rev. Cancer* **15**, 397-408. doi:10.1038/nrc3960

Sherr, C. J. and Roberts, J. M. (1999). CDK inhibitors: positive and negative regulators of G1-phase progression. *Genes Dev.* **13**, 1501-1512. doi:10.1101/gad.13.12.1501

Sobecki, M., Mrouj, K., Colinge, J., Gerbe, F., Jay, P., Krasinska, L., Dulic, V. and Fisher, D. (2017). Cell-cycle regulation accounts for variability in Ki-67 expression levels. *Cancer Res.* **77**, 2722-2734. doi:10.1158/0008-5472.CAN-16-0707

Stein, G. H., Drullinger, L. F., Soulard, A. and Dulić, V. (1999). Differential roles for cyclin-dependent kinase inhibitors p21 and p16 in the mechanisms of senescence and differentiation in human fibroblasts. *Mol. Cell. Biol.* **19**, 2109-2117. doi:10.1128/MCB.19.3.2109

Stolz, A., Ertych, N. and Bastians, H. (2011). Tumor suppressor CHK2: regulator of DNA damage response and mediator of chromosomal stability. *Clin. Cancer Res.* **17**, 401-405. doi:10.1158/1078-0432.CCR-10-1215

Stracker, T. H., Couto, S. S., Cordon-Cardo, C., Matos, T. and Petrini, J. H. J. (2008). Chk2 suppresses the oncogenic potential of DNA replication-associated DNA damage. *Mol. Cell* **31**, 21-32. doi:10.1016/j.molcel.2008.04.028

Sturmlechner, I., Zhang, C., Sine, C. C., van Deursen, E.-J., Jeganathan, K. B., Hamada, N., Grasic, J., Friedman, D., Stutchman, J. T., Can, I. et al. (2021). p21 produces a bioactive secretome that places stressed cells under immunosurveillance. *Science* **374**, 577-581. doi:10.1126/science.abb3420

Topacio, B. R., Zatulovskiy, E., Cristea, S., Xie, S., Tambo, C. S., Rubin, S. M., Sage, J., Kõivomägi, M. and Skotheim, J. M. (2019). Cyclin D-Cdk4,6 drives cell-cycle progression via the retinoblastoma protein's C-terminal helix. *Mol. Cell* **74**, 758-770.e4. doi:10.1016/j.molcel.2019.03.020

Ullah, Z., de Renty, C. and DePamphilis, M. L. (2011). Checkpoint kinase 1 prevents cell cycle exit linked to terminal cell differentiation. *Mol. Cell. Biol.* **31**, 4129-4143. doi:10.1128/MCB.05723-11

Yang, K., Hitomi, M. and Stacey, D. W. (2006). Variations in cyclin D1 levels through the cell cycle determine the proliferative fate of a cell. *Cell Div.* **1**, 32. doi:10.1186/1747-1028-1-32

Yang, C., Li, Z., Bhatt, T., Dickler, M., Giri, D., Scaltriti, M., Baselga, J., Rosen, N. and Chandarlapaty, S. (2017a). Acquired CDK6 amplification promotes breast cancer resistance to CDK4/6 inhibitors and loss of ER signaling and dependence. *Oncogene* **36**, 2255-2264. doi:10.1038/onc.2016.379

Yang, H. W., Chung, M., Kudo, T. and Meyer, T. (2017b). Competing memories of mitogen and p53 signalling control cell-cycle entry. *Nature* **549**, 404-408. doi:10.1038/nature23880

Yosef, R., Pilpel, N., Papismadov, N., Gal, H., Ovadya, Y., Vadai, E., Miller, S., Porat, Z., Ben-Dor, S. and Krizhanovsky, V. (2017). p21 maintains senescent cell viability under persistent DNA damage response by restraining JNK and caspase signaling. *EMBO J.* **36**, 2280-2295. doi:10.15252/embj.201695553

Yuan, R., Vos, H. R., van Es, R. M., Chen, J., Burgering, B. M. T., Westendorp, B. and de Bruin, A. (2018). Chk1 and 14-3-3 proteins inhibit atypical E2Fs to prevent a permanent cell cycle arrest. *EMBO J.* **37**, e97877. doi:10.15252/embj.201797877

Zhang, Y.-W., Otterness, D. M., Chiang, G. G., Xie, W., Liu, Y.-C., Mercurio, F. and Abraham, R. T. (2005). Genotoxic stress targets human Chk1 for degradation by the ubiquitin-proteasome pathway. *Mol. Cell* **19**, 607-618. doi:10.1016/j.molcel.2005.07.019

Zhang, L., Geng, X., Wang, F., Tang, J., Ichida, Y., Sharma, A., Jin, S., Chen, M., Tang, M., Pozo, F. M. et al. (2022). 53BP1 regulates heterochromatin through liquid phase separation. *Nat. Commun.* **13**, 360. doi:10.1038/s41467-022-28019-y